

Efficient Decision Trees for Tensor Regressions

Hengrui Luo

Department of Statistics, Rice University;

Computational Research Division, Lawrence Berkeley National Laboratory

and

Akira Horiguchi

Department of Statistics, University of California Davis

and

Li Ma

Department of Statistics, University of Chicago

Abstract

We proposed the tensor-input tree (TT) method for scalar-on-tensor and tensor-on-tensor regression problems. We first address scalar-on-tensor problem by proposing scalar-output regression tree models whose input variables are tensors (i.e., multi-way arrays). We devised and implemented fast randomized and deterministic algorithms for efficient fitting of scalar-on-tensor trees, making TT competitive against tensor-input GP models (Sun et al., 2023; Yu et al., 2018). Based on scalar-on-tensor tree models, we extend our method to tensor-on-tensor problems using additive tree ensemble approaches. Theoretical justification and extensive experiments, including testing robustness to entrywise input tensor noise, are provided on real and synthetic datasets to illustrate the performance of TT.

Our implementation is provided at <http://www.github.com/hrluo>.

Keywords: Decision tree regressions, scalar-on-tensor regressions, tensor-on-tensor regressions, ensemble methods.

1 Introduction

1.1 Problem and Settings

In recent years, the intersection of tensor data analysis and non-parametric modeling methods (Guhaniyogi et al., 2017; Papadogeorgou et al., 2021; Wang and Xu, 2024) has garnered considerable interest among mathematicians and statisticians. Non-parametric tensor models have the potential to handle complex multi-dimensional data (Bi et al., 2021) and represent spatial correlation between entries of data. This paper addresses both scalar-on-tensor (i.e., to predict a scalar response based on a tensor input) and tensor-on-tensor (i.e., both the input and output are tensors) non-linear regression problems using recursive partitioning methods, often referred to as tree(-based) models.

Supervised learning on tensor data, such as tensor regression, has significant relevance due to the proliferation of multi-dimensional data in modern applications. Tensor data naturally arises in various fields such as imaging (Wang and Xu, 2024), neuroscience (Li et al., 2018), and computer vision (Luo and Ma, 2025), where observations often take the form of multi-way arrays. Traditional regression models typically handle vector inputs and outputs, and thus can fail to capture the structural information embedded within tensor data.

Tree-based methods (Breiman et al., 1984; Breiman, 2001; Friedman et al., 2004; Hastie et al., 2009), on the other hand, offer a flexible and interpretable framework for regression. They can capture non-linear relationships and interactions between features, making them particularly well-suited for the intricate nature of tensor data. The ability to apply tree models directly to tensor inputs provides a powerful tool for researchers and practitioners dealing with high-dimensional and multi-way data.

Existing tree regression methods like CART, random forest, and boosting do not handle tensor data’s multi-array characteristics. We develop regression tree models for tensor inputs and outputs to enable non-linear and possibly non-parametric modeling that captures complex tensor interactions. We introduce scalar-on-tensor regression with new scalar-output tree algorithms featuring strategies and loss functions designed for tensor data, integrating low-rank tensor approximation methods.

We then address the tensor-on-tensor problem by constructing an additive tree ensemble model analogous to that for tree boosting in regression (Chipman et al., 1998; Denison et al., 1998; Friedman, 2001; Friedman et al., 2004). Our tensor tree boosting uses our scalar-on-tensor tree models as “weak” learners to achieve competitive predictive performance. We show that the tree ensemble approach is particularly effective for complex outcome spaces such as in tensor-response regression.

In addition to developing methodology, we also address the computational scalability and

basic theoretical guarantees of our algorithms. This is particularly important in the ensemble approach, as a large number of single trees are trained. Our algorithms are competitive with existing tensor regression approaches such as tensor Gaussian processes (Yu et al., 2018; Sun et al., 2023), and alternative non-parametric models. Non-parametric tree-based models provide appropriate data partitions in conjunction with ensemble methods to extend these models into the domain of tensor inputs and outputs, integrating methodological ideas and theories from tensor decompositions and low-rank approximations in parametric tensor regression models (Zhou et al., 2013; Li and Zhang, 2017; Li et al., 2018). Our proposed non-parametric regression method of *tensor-input trees* (TT) allows us to capture multi-way dependence expressed in tensor covariates, and presents a scalable model for potentially heterogeneous tensors. In contrast to smoothing methods, TT is particularly suitable when there are non-smooth or change-of-pattern behavior in the tensor.

In connection with generalized tree-based models with inputs in Fréchet spaces (Capitaine et al., 2024) (a.k.a., Fréchet trees in Qiu et al. (2024)), the tensor space can be viewed as a Fréchet space with additional structure that admits unique moments (Luo and Ma, 2025) and low-rank decompositions (Kolda and Bader, 2009). This allows us to introduce novel tensor-specific splitting rules (i.e., LAE and LRE in Sec 2.1), whereas existing works (Capitaine et al., 2024; Qiu et al., 2024) only consider a variance-based splitting criteria using clustering following the spirit of honest forest (Athey et al., 2019). In light of this, Krawczyk (2021) developed a clustering-based splitting tensor-input tree model. To reduce the computational burden introduced by solving Fréchet moments in splitting, Bulté and Sørensen (2024) propose to solve the optimization among a smaller fraction of solution space called Fréchet Medoid, which is very similar to our subsampling method, but different from our branch-and-bound strategy. In addition to single tensor-input trees, we also leverage boosting ensembles (Friedman, 2001) in order to reduce bias in tensor-output cases; in contrast, a random forest approach leaves the bias unchanged and instead aims to reduce variance.

1.2 Regression Trees Revisited

We start by reviewing a scalar-on-vector regression problem. Consider the regression setup with n data pairs (X_i, y_i) where the input and response variables are $X_i \in \mathbb{R}^d, y_i \in \mathbb{R}$

$$y_i = f(X_i) + \epsilon_i, i = 1, \dots, n \quad (1)$$

where $f: \mathbb{R}^d \rightarrow \mathbb{R}$ is a real-valued function and the ϵ_i s are independent mean zero noises.

A single regression tree assumes a vector input in \mathbb{R}^d and is built by recursively partitioning (Breiman et al., 1984; Hastie et al., 2009) the input space into disjoint regions

$R_1, R_2, \dots, R_J \subset \mathbb{R}^d$, $R_j \cap R_k = \emptyset$ when $j \neq k$, before fitting a regression mean model m_j in each region. The regression tree model can be written as

$$y_i = g(X_i) + \epsilon_i, \quad g(X; \mathcal{T}, \mathcal{M}) = \sum_{j=1}^J m_j(X) \cdot I(X \in R_j), \quad (2)$$

where $I(X \in R_j)$ is an indicator function, \mathcal{T} is the tree structure that dictates the partition of the input space, and \mathcal{M} determines the tree model's prediction values. The partition is created by minimizing a splitting criterion such as the sum of squared residuals (or sum of variances) of responses within each region:

$$\text{SSE}(\mathcal{T}; y_1, \dots, y_n) = \sum_{j=1}^J \frac{1}{N_j} \sum_{X_i \in R_j} (y_i - \hat{y}_{R_j})^2. \quad (3)$$

Typically $J = 2$ so that each tree split creates left and right children nodes which correspond to two (sub)regions defined by bisecting a given region along the j_1 th axis at the observed $\mathbf{X}[j_0, j_1]$, i.e., at the (j_0, j_1) -th entry in the design matrix $\mathbf{X} \in \mathbb{R}^{n \times d}$ created by stacking the vectors X_1, \dots, X_n as rows. We adopt a top-down greedy algorithm using criterion (3) (see Algorithm 2) to create the partition. The model then assigns a prediction value to each region; this value is often the sample mean of the responses of the training data in the region, i.e., $m_j(X) = \hat{y}_{R_j}$ where $\hat{y}_{R_j} = \frac{1}{N_j} \sum_{i=1}^n y_i \cdot I(X_i \in R_j)$ and $N_j = \sum_{i=1}^n I(X_i \in R_j)$.

While there exists Bayesian regression tree methods (Chipman et al., 1998; Denison et al., 1998; Chipman et al., 2010, 2012), this paper will focus on non-Bayesian approaches of ensemble construction, but generalizing our model to Bayesian models is natural in most scenarios (Wang and Xu, 2024).

1.3 Tensor Input Linear Regression

Instead of adopting a constant baseline, which ignores any further dependence between the outcome and predictors, our base model will use existing linear regression models tailored for tensor inputs. The more flexible baseline model will not only improve predictive performance, but it will also generally lead to more parsimonious trees and therefore improve computational efficiency.

Next we briefly review the relevant tensor-input linear models considered later as base models. When the regression function f in (1) is assumed to be linear, we can fit a *vector-input linear regression model* for estimation and prediction of the output y . In matrix product notation, this model is $\mathbf{y} = \mathbf{X}\boldsymbol{\beta} + \boldsymbol{\epsilon}$ with $\mathbf{X} \in \mathbb{R}^{n \times d}$ and $\mathbf{y} \in \mathbb{R}^{n \times 1}$. We can estimate the

model by solving the loss function (i.e., L_2 residual) $\|\mathbf{y} - \mathbf{X}\boldsymbol{\beta}\|_2$ for the coefficient $\boldsymbol{\beta} \in \mathbb{R}^{d \times 1}$. This can be generalized to *tensor-input (multi-)linear regression* with a tensor input and a scalar response (Zhou et al., 2013; Luo and Ma, 2025). Without loss of generality, we consider data pairs consisting of a 3-way input tensor $\mathbf{X}_i \in \mathbb{R}^{1 \times d_1 \times d_2}$, where the first dimension is an observation index as in vector-input models, and a scalar response $y_i \in \mathbb{R}^1$. This setup can directly handle tensor inputs via the tensor product \circ in the tensor regression model:

$$y_i = \mathbf{X}_i \circ \mathbf{B} + E_i, \quad i = 1, \dots, n, \quad (4)$$

where the matrix $\mathbf{y} \in \mathbb{R}^{n \times 1}$ stacks the responses y_1, \dots, y_n , the tensor $\mathbf{B} \in \mathbb{R}^{d_1 \times d_2}$ collects the regression coefficients, and the tensor $\mathbf{E} \in \mathbb{R}^{n \times 1}$ stacks the i.i.d. Gaussian noise $E_i \in \mathbb{R}^1$. The tensor products are defined as $\mathbf{X} \circ \mathbf{B} = \sum_i^n \sum_{j_1}^{d_1} \sum_{j_2}^{d_2} \mathbf{X}[i, j_1, j_2] \mathbf{B}[j_1, j_2]$ in Zhou et al. (2013); Guo et al. (2011) (Eq. (5)) but the assumed model (4) is compatible with other tensor products as well. As in the vector-input case, the solution to (4) corresponds to the least-squares problem $\min_{\mathbf{B}^{(n)}} \|\mathbf{y}^{(n)} - \mathbf{X}^{(n)} \circ \mathbf{B}^{(n)}\|_2$. In this paper, the superscript (n) will denote an object created by stacking n quantities (corresponding to n observations) along the first dimension. For $\mathbf{X}^{(n)}$ we stack all n samples; for $\mathbf{B}^{(n)}$ the shared coefficient \mathbf{B} is simply repeated n times. If it is obvious that the object is stacked, we will omit the superscript.

As Zhou et al. (2013) and Li et al. (2018) noted, scalar-on-tensor linear regression can extend to D -mode tensor inputs $\mathbf{X} \in \mathbb{R}^{n \times d_1 \times d_2 \times \dots \times d_D}$ with more complex notations. We focus on $D = 3$ and $D = 4$ (i.e., $\mathbf{X} \in \mathbb{R}^{n \times d_1 \times d_2}$ and $\mathbf{X} \in \mathbb{R}^{n \times d_1 \times d_2 \times d_3}$), which are common in applications, with notation centered on $D = 3$. The model (4) has high-dimensional coefficients \mathbf{B} complicating model fitting and optimization. Current state-of-the-art implementations like CatBoost (Prokhorenkova et al., 2018) and XGBoost (Chen and Guestrin, 2016) support up to $D = 2$ and overlook spatial correlation in $\mathbf{X} \circ \mathbf{B}$. We use the state-of-the-art **tensorly** (Kossaifi et al., 2019) implementation for scalar-on-tensor CP/Tucker regressions for leaf models in our tree regression method.

Tensor decomposition (Kolda and Bader, 2009; Johndrow et al., 2017) is a popular approach to reduce dimensionality and hence model complexity by aiming to capture multi-way interactions in the data using lower-dimensional representations. In particular, CP and Tucker decompositions extend the idea of low-rank approximation (e.g., SVD) from matrices to tensors, offering unique ways to explore and model the possible sparse structure in tensors. *CP decomposition* represents a tensor $\mathbf{T} \in \mathbb{R}^{t_1 \times t_2 \times t_3}$ as a linear combination of R rank-1 tensors $\mathbf{a}_r \times \mathbf{b}_r \times \mathbf{c}_r$:

$$\mathbf{T} = \sum_{r=1}^R \lambda_r \mathbf{a}_r \times \mathbf{b}_r \times \mathbf{c}_r \quad (5)$$

where \times denotes the outer product (i.e., Kronecker product) between vectors, and λ_r is the scalar weight of the r -th component for *factor vectors* $\mathbf{a}_r \in \mathbb{R}^{t_1}$, $\mathbf{b}_r \in \mathbb{R}^{t_2}$, $\mathbf{c}_r \in \mathbb{R}^{t_3}$, reducing the number of coefficients in \mathbf{B} from nd_1d_2 to $R(1+t_1+t_2+t_3) \leq R(1+n+d_1+d_2)$. *Tucker decomposition* represents the tensor \mathbf{T} using a (usually dense) core tensor $\mathbf{G} \in \mathbb{R}^{R_1 \times R_2 \times R_3}$, and factor matrices $\mathbf{A}_1 \in \mathbb{R}^{R_1 \times t_1}$, $\mathbf{A}_2 \in \mathbb{R}^{R_2 \times t_2}$, $\mathbf{A}_3 \in \mathbb{R}^{R_3 \times t_3}$ where $R_1 \leq t_1$, $R_2 \leq t_2$, $R_3 \leq t_3$:

$$\mathbf{T} = \mathbf{G} \times_1 \mathbf{A}_1 \times_2 \mathbf{A}_2 \times_3 \mathbf{A}_3 = \sum_{r_1=1}^{R_1} \sum_{r_2=1}^{R_2} \sum_{r_3=1}^{R_3} \lambda_{r_1, r_2, r_3} \mathbf{a}_{r_1} \times \mathbf{b}_{r_2} \times \mathbf{c}_{r_3}. \quad (6)$$

Here \times_q denotes the *product along mode- q* ($q = 1, 2, \dots, D$), which is the multiplication of a tensor by another tensor along a specific mode by permuting the mode- q in front and permuting it back. That is, we pull one dimension to the front, flatten it, transform it by a matrix, then put everything back the way it was, except that the numbers along one dimension are mixed and changed (Kolda and Bader, 2009). The core tensor \mathbf{G} has rank (R_1, R_2, R_3) along each mode but is typically much smaller in size than \mathbf{T} . We use the second equivalent summation as in (3) of Li et al. (2018) for $\lambda_{r_1, r_2, r_3} \in \mathbb{R}$, $\mathbf{a}_{r_1} \in \mathbb{R}^{t_1}$, $\mathbf{b}_{r_2} \in \mathbb{R}^{t_2}$, $\mathbf{c}_{r_3} \in \mathbb{R}^{t_3}$, reducing the number of coefficients parameters from nd_1d_2 to $(1+t_1R_1+t_2R_2+t_3R_3) \leq (1+nR+d_1R+d_2R)$ when we use the same rank R along each mode.

For tensor regression (4), we adopt a low-rank decomposition for the coefficient \mathbf{B} using CP or Tucker decompositions and use the factor matrices through the linear model (4), following the state-of-the-art practice in Li et al. (2018); Zhou et al. (2013).

Organization. The rest of the paper is organized as follows: Section 2 introduces the ingredients for fitting a single tree model with tensor inputs, including a discussion of splitting criteria and complexity-based pruning. Section 3 reviews ensemble techniques for improving single trees before introducing entry-wise and low-rank methods for handling tensor output using ensembles (Section 3.1). Section 4 provides two groups of theoretical results including the consistency of leaf models and the oracle bounds for predictions. Section 5 investigates the effect of using novel splitting criteria (Section 5.1), compares to other tensor models in terms of prediction and efficiency (Section 5.2), and concludes with a tensor-on-tensor application example (Section 5.3). Section 6 provides discussions and future works. The Supplementary Material contains additional simulation experiments, including for robustness to entrywise input noise, and for comparing to existing random-forest methods.

2 Trees for Tensor Inputs

We now propose and implement fast algorithms for the scalar-on-tensor regression problem

$$y_i = g^*(\mathbf{X}_i) + E_i, i = 1, \dots, n \quad (7)$$

for inputs $\mathbf{X}_i \in \mathbb{R}^{d_1 \times d_2}$ and responses $y_i \in \mathbb{R}$. Here $g^* : \mathbb{R}^{d_1 \times d_2} \rightarrow \mathbb{R}$ is a real-valued function we wish to estimate and the E_i s are independent mean zero noises. Extending the tree model (2) and creating ensembles for tensor input regression require ingredients from low-rank tensor approximations (i.e., (5) and (6)) and associated low-rank tensor input regressions.

2.1 Splitting Criterion

For continuous vector inputs, the split rule $\mathbf{X}[:, j_1] > c$ in (2) and Algorithm 2 can be written as the rule $\mathbf{X}^\top \mathbf{e}_{j_1} > c$ using the design matrix \mathbf{X} and unit vector \mathbf{e}_{j_1} along splitting coordinate j_1 . For continuous *tensor* inputs, we can consider the split rule $\mathbf{X} \circ \mathbf{e}_{j_1, j_2} > c$ and the following splitting criteria:

Variance criterion (SSE). Under this criterion, which generalizes the well-accepted criterion (3) in the tree regression literature (Breiman et al., 1984) to scalar-on-tensor regressions (7), we choose a dimension pair (j_1, j_2) and observed value $\mathbf{X}[j_0, j_1, j_2]$ so that the induced pair of children

$$R_1 := \{\mathbf{X} \mid \mathbf{X}[:, j_1, j_2] \leq \mathbf{X}[j_0, j_1, j_2]\} \quad R_2 := \{\mathbf{X} \mid \mathbf{X}[:, j_1, j_2] > \mathbf{X}[j_0, j_1, j_2]\} \quad (8)$$

minimizes the sum of variances (here $I_j := \{i \mid \mathbf{X}[i, j_1, j_2] \in R_j\}$ and $\mathbf{y}[I_j, :] = \{y_i \mid i \in I_j\}$)

$$\text{SSE}(j_0, j_1, j_2) = \sum_{j=1}^2 \frac{1}{N_j} \sum_{\mathbf{X}_i \in R_j} (y_i - \hat{y}_{R_j})^2 = \sum_{j=1}^2 \frac{1}{N_j} \left\| \mathbf{y}[I_j, :] - \frac{1}{|I_j|} \mathbf{1}_{|I_j|}^\top \mathbf{y}[I_j, :] \cdot \mathbf{1}_{|I_j|} \right\|_2^2 \quad (9)$$

over all such possible pairs of children.

Low-rank approximation error (LAE). This criterion aims to partition the input space by leveraging the potential low-rank structure in the tensor input \mathbf{X} . Rather than use the predictors, we can split based on how closely the children tensor inputs match their low-rank CP or Tucker approximations. Namely, we choose the child pair (8) whose tensor inputs $\mathbf{X}[I_j, :, :] \in \mathbb{R}^{|I_j| \times d_1 \times d_2}$ (for $j = 1, 2$) and corresponding tensor low-rank approximations

$\widetilde{\mathbf{X}}[I_j, :, :]$ minimize the error (again, here $I_j := \{i \mid \mathbf{X}[i, j_1, j_2] \in R_j\}$)

$$\text{LAE}(j_0, j_1, j_2) = \sum_{j=1}^2 \sum_{i \in I_j} \left\| \widetilde{\mathbf{X}}[i, :, :] - \mathbf{X}[i, :, :] \right\|_F^2 \quad (10)$$

among all possible such child pairs. This criterion does not use the predictors \mathbf{y} and is more expensive to compute than (9) as described by Lemma 1 and 2 below.

Low-rank regression error (LRE). Alternatively, we can find a split that minimizes the low-rank *regression* error in each child:

$$\text{LRE}(j_0, j_1, j_2) = \sum_{j=1}^2 \sum_{i \in I_j} \left\| \widetilde{\mathbf{y}}(\mathbf{X}[i, :, :]) - y_i \right\|_F^2, \quad (11)$$

where $\widetilde{\mathbf{y}}(\mathbf{X}[I_j, :, :])$ is the chosen CP (5) or Tucker (6) low-rank regression model (of a given target rank) of $\mathbf{X}[I_j, :, :]$ against $\mathbf{y}[I_j]$. Intuitively, this minimizes the error of predicting \mathbf{y} in each child, which is analogous to CART minimizing the sum of variances of \mathbf{y} in each node. Because we fit two models for two children nodes, (11) is slightly more expensive than (10). Any given split with $D = 3$ requires a split-coordinate pair (j_1, j_2) and index j_0 for the split value $c = \mathbf{X}[j_0, j_1, j_2]$. The j_0, j_1, j_2 triplet is usually obtained by solving the following mixed integer problem of dimensionality nd_1d_2 :

$$\min_{(j_0, j_1, j_2) \in \{1, \dots, n\} \times \{1, \dots, d_1\} \times \{1, \dots, d_2\}} \mathcal{L}(j_0, j_1, j_2) \quad (12)$$

where the criterion function \mathcal{L} is chosen as one of (9), (10) or (11). This is a major computational overhead for generating a tree structure via (binary) splitting.

The splitting criteria SSE and LRE involve both \mathbf{X} and \mathbf{y} , whereas LAE is specifically designed for low-rank tensors \mathbf{X} (or mat-vec that essentially has low-rank structures). Because LAE does not involve the response \mathbf{y} , the learned tree based on LAE will well approximate the mean response only when the underlying latent tree structure in \mathbf{X} corresponds to that in \mathbf{y} . On the other hand, SSE and LRE more directly target the prediction task and more easily produce a good fit to the data, but also make the algorithm more prone to overfitting, though this issue can be easily addressed with proper regularization techniques such as pruning and out-of-sample validation.

The key idea behind the LRE loss is to incorporate low-rank tensor regression as the baseline models on the leaves of a partition tree. Trees can capture non-linear local structures in the underlying mean functions but are ineffective at approximating global smooth structures such as linear patterns on some latent dimensions which low-rank tensor regression

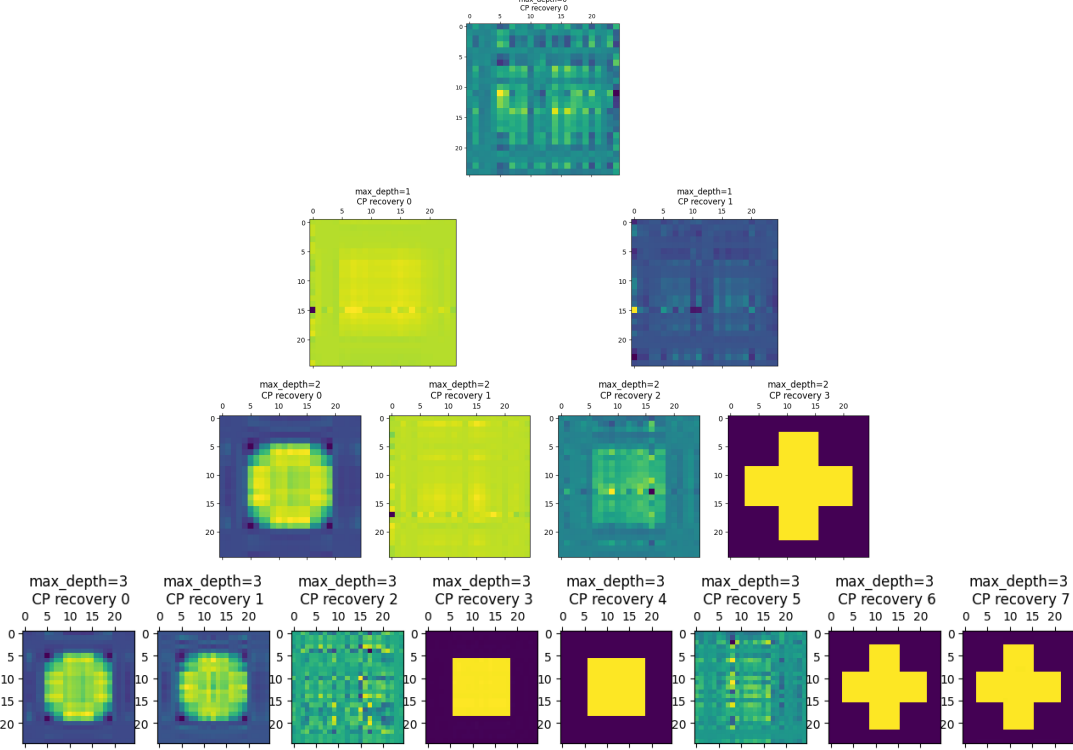


Figure 1: Tensor-input decision tree regression estimated coefficients $\hat{\mathbf{B}}$ on a mixture-of-classes model ($\tau = 0.1$) with rank-2 CP regression at leaf models from the circle-rectangle-cross example in Zhou et al. (2013). Each row corresponds to a $\text{max_depth} \in \{0, 1, 2, 3\}$.

targets. As such, we construct trees using novel splitting criteria and complexity measures, then fit tensor regressions at each leaf node. To show the effectiveness of our model, we first generate three classes of coefficient tensors $\mathbf{B}_1, \mathbf{B}_2, \mathbf{B}_3$, and then simulate i.i.d. Gaussian tensors \mathbf{X}_i to yield the response $\mathbf{y}_i = \mathbf{X}_i \circ \mathbf{B}_i + \delta_i$ for each class, where the elements of δ_i are independent shifted noises $N(i, \sigma^2)$ to ensure identifiability between these three classes. Figure 1 shows a scenario of mixed class data (Zhou et al., 2013) in which existing tensor regressions (i.e., the top row) fail to recover each class but a *tree*-based regression model is successful with appropriate splits. In addition, this tree-based model can realize typical low-rank CP and Tucker regression models as special cases when the max depth of the tree is set to be zero (i.e., when the tree has only one node) and the only model is a single low-rank regression model. The effects of the splitting and pruning criteria will be further investigated in Section 5.1 and Appendix D.

As a final note, the variance and LRE splitting criteria can be used to tackle a regression problem with a tensor response and vector predictor. On the other hand, a CP or Tucker decomposition of a vector predictor is just the predictor itself, so the LAE error would be zero for any pair of potential children and hence cannot be used with a vector predictor.

Algorithm 1: Exhaustive search method for fitting tensor-input decision tree regressor with low-rank splitting criteria (10) and (11).

Result: Train a tensor-input single decision tree regressor with exhaustive search

- 1 **Function** $\text{fit}(\mathbf{X} \in \mathbb{R}^{n \times d_1 \times d_2}, \mathbf{y} \in \mathbb{R}^n)$:
- 2 **begin**
- 3 Initialize root node. **for** $node$ in $tree$ **do**
- 4 Calculate for all potential splits along each dimension pair (j_1, j_2) : Find $\arg \min_{j_0 \in \{1, \dots, n\}, j_1 \in \{1, \dots, d_1\}, j_2 \in \{1, \dots, d_2\}} \text{LAE}(j_0, j_1, j_2)$ or $\text{LRE}(j_0, j_1, j_2)$;
- 5 With the minimizer (j_0^*, j_1^*, j_2^*) , split the dataset on the chosen dimension pair (j_1^*, j_2^*) and split value $\mathbf{X}[j_0^*, j_1^*, j_2^*]$, creating left and right child nodes using data in R_1, R_2 ;
- 6 **end**
- 7 Fit the chosen mean/CP/Tucker models at each of the leaf nodes.
- 8 **end**

2.2 Reducing Computational Cost

There are two major computational overheads in fitting the tree tensor regression model we just proposed: leaf model fitting and splitting criteria computation. The cost of the former is alleviated by the tree structure providing a partitioning regime that allows divide-and-conquer scaling. The latter, however, is a new computational challenge born from the nature of tensor data as we explain below.

It is computationally very expensive to exhaustively search (see Algorithm 1) for the best split node in tensor-input decision trees. This process evaluates all possible splits along each dimension pair (j_1, j_2) , which requires examining every combination of j_0 , j_1 , and j_2 . Consequently, the search space size for each split decision is $n \cdot d_1 \cdot d_2$, which scales poorly with increasing dataset size and tensor dimensions, making exhaustive search computationally intensive and impractical for large-scale data or real-time applications.

In addition, the computational complexity of (10) and (11) is rather high since both CP and Tucker decompositions rely on expensive alternating algorithms, which often have convergence issues. Therefore, the greedy search approach over a space of size $d_1 d_2$ to solve $\min_{(j_0, j_1, j_2)} \mathcal{L}(j_0, j_1, j_2)$ is no longer an efficient algorithmic design, given the frequency of splitting in fitting a regression tree structure.

Splitting criteria complexity analysis. Computing the variance in (9) for scalar responses has complexity $\mathcal{O}(n)$, which can be vectorized and does not scale with dimensions. On the other hand, the complexities of (10) and (11) are dominated by the CP and Tucker decomposition of the coefficient tensors. Although many scalable methods are proposed for CP and Tucker decompositions, the well-adopted alternating least square (ALS) (Malik and

Becker, 2018) solvers are of iterative nature and hence can have relatively high complexities:

Lemma 1. (*CP-ALS per iteration complexity Minster et al. (2023) Section 3.2*) *In the alternating least square algorithm for the rank- R CP decomposition of a $n \times d_1 \times d_2 \times \cdots \times d_K$ tensor where $R < n$ and $R \ll d_i, i = 1, \dots, K$, each iteration has time complexity $\mathcal{O}((K+1) \cdot \prod_{i=1}^K d_i \cdot R)$. Therefore, for N^* iterations in CP-ALS, the overall complexity is bounded from above by $\mathcal{O}(N^* \cdot (K+1)R \cdot (\max_i d_i)^K)$.*

Lemma 2. (*Tucker-ALS per iteration complexity Oh et al. (2018) Section II.C*) *In the alternating least square algorithm for the rank- $(R, d'_1, d'_2, \dots, d'_K)$ (i.e., core tensor dimension) Tucker decomposition of a $n \times d_1 \times d_2 \times \cdots \times d_K$ tensor, each iteration has complexity*

$$\mathcal{O} \left(\min \left\{ n \prod_{j=1}^K d_j'^2, n^2 \prod_{j=1}^K d_j' \right\} + \sum_{i=1}^K \min \left\{ R^2 \cdot d_i \prod_{j \neq i} d_j'^2, R \cdot d_i^2 \prod_{j \neq i} d_j' \right\} \right).$$

When $R < n$ and $d'_i \asymp d_i \ll n, i = 1, \dots, K$, for N^* iterations in Tucker-ALS, the overall complexity is at most $\mathcal{O}(N^* \cdot n \cdot (\max_i d_i)^{2K})$.

To simplify our subsequent analysis, we assume $n \asymp R$ and always choose a constant maximal iteration number N^* regardless of the convergence. Then both decompositions have time complexities at most $\mathcal{O}(N^* \cdot n \cdot (\max_i d_i)^{2K})$ which scales linearly with n . However, the factor $N^* \cdot (\max_i d_i)^{2K}$ greatly increases complexity in greedy-style tree-fitting.

Adoption of mean splitting values. Minimizing these three criteria can be a strategy to choose the split-value index j_0 and splitting coordinates (j_1, j_2) , and can easily generalize to regression trees for tensor inputs. Finding the best combination of (j_0, j_1, j_2) using (3), (10), (11), in a worst-case scenario, needs $n \cdot \prod_{j=1}^K d_j$ -many variance evaluations and contributes to a quadratic complexity in n . But if we do not optimize over j_0 and instead split on the sample mean $m_{j_1, j_2} := \frac{1}{n} \sum_{i=1}^n \mathbf{X}[i, j_1, j_2]$, we can simplify the partitions in (3), (10), (11) as:

$$\bar{R}_1 := \{\mathbf{X} \mid \mathbf{X}[:, j_1, j_2] \leq m_{j_1, j_2}\}, \quad \bar{R}_2 := \{\mathbf{X} \mid \mathbf{X}[:, j_1, j_2] > m_{j_1, j_2}\}. \quad (13)$$

Since we no longer need to determine j_0 , we can complete the search within linear time in n , without losing too much empirical prediction performance. Then the corresponding loss

functions in our reduced optimization problems become (here $I_j := \{i \mid \mathbf{X}[i, j_1, j_2] \in \bar{R}_j\}$):

$$\overline{\text{SSE}}(j_1, j_2) = \sum_{j=1}^2 \frac{1}{|I_j|} \sum_{i \in I_j} \|\hat{y}_{\bar{R}_j} - y_i\|_2^2, \quad (14)$$

$$\overline{\text{LAE}}(j_1, j_2) = \sum_{j=1}^2 \sum_{i \in I_j} \left\| \widetilde{\mathbf{X}}[i, :, :] - \mathbf{X}^{(n)}[i, :, :] \right\|_F^2, \quad (15)$$

$$\overline{\text{LRE}}(j_1, j_2) = \sum_{j=1}^2 \sum_{i \in I_j} \left\| \widetilde{\mathbf{y}}(\mathbf{X}^{(n)}[i, :, :]) - y_i \right\|_F^2. \quad (16)$$

Removing the search along the first mode shrinks the dimensionality of the optimization problem $\min_{(j_0, j_1, j_2)} \mathcal{L}(j_0, j_1, j_2)$ to reduce the complexity per evaluation of the split criterion.

Figure 2 shows that the loss functions LAE and LRE lead to similar complexities and predictive behavior. Although both losses are based on low-rank tensor decomposition, LRE (like SSE) focuses on the children's predictive loss. In what follows, we mainly study TT models with LRE in (11) or its mean version (16) as our default loss functions, unless otherwise stated. Appendix B details two advanced searching techniques, namely leverage score sampling (LS) and branch-and-bound (BB) methods for even more efficient searches.

In the spirit of Lemma 11 of Luo and Pratola (2022) and the above Lemmas 1 and 2, we can derive the per-iteration complexity (of ALS used for computing CP and Tucker decompositions) by observing that there are $\mathcal{O}(n \log k)$ evaluations of the loss function in a tree with k nodes ($\log k$ layers) and $n \geq 1$ sample points:

Proposition 1. *(Computational complexity for TT) If there are $n \geq 1$ samples with at most k nodes for the splitted tree structure and no more than $N^* < \infty$ iterations for all decompositions, the worst-case computational complexity for generating this tree structure (via exhaustive search for problem (12)) is*

- (1) $\mathcal{O}(nd_1d_2 \log k)$ if the loss function is (9).
- (2) $\mathcal{O}(n^2d_1^2d_2^2 \log k)$ if the loss function is (10) or (15) with CP low-rank approximations.
- (3) $\mathcal{O}(n^2d_1^2d_2^2 \cdot [\min(d_1d_2, n) + \min(d_1, d_2)] \log k)$ if the loss function is (11) or (16) with Tucker low-rank approximations.

Proof. See Appendix F. □

This complexity result indicates that the tensor tree model has $\mathcal{O}(n^2 \cdot C)$ complexity (where $C = C(d_1, d_2)$ depends on the dimensionality of the tensor inputs) compared to the larger $\mathcal{O}(n^3)$ complexity (whose constant inside big O also depends on the kernel evaluation) incurred by tensor GP models (Yu et al., 2018) as shown later in Figure 6. We can also see

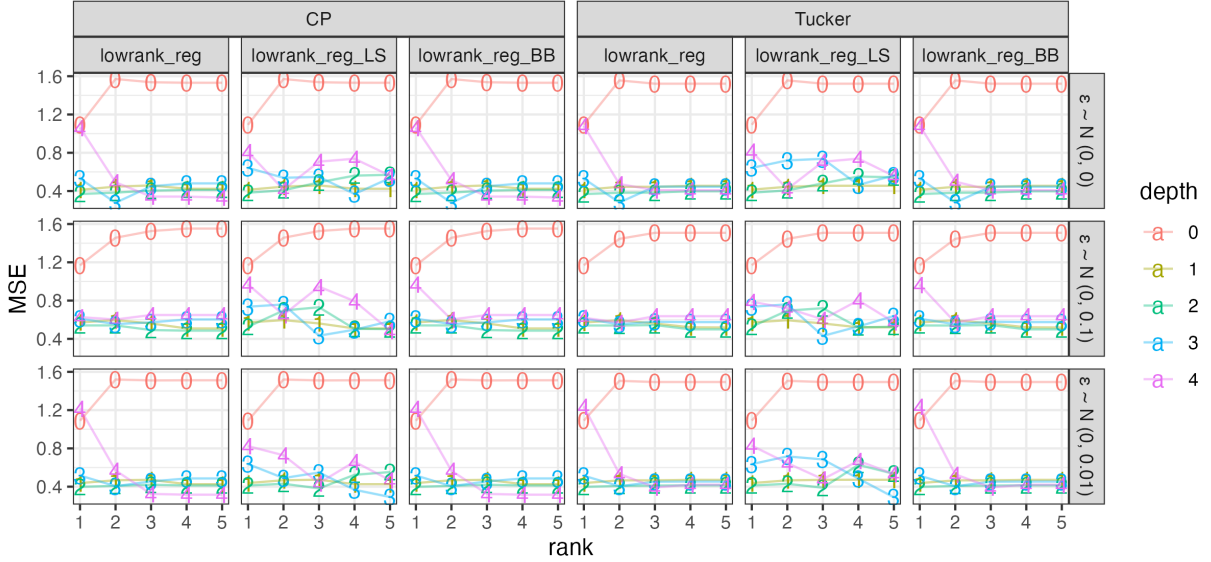


Figure 2: Out-of-sample MSEs for tree regression models of different maximal depths, using a $(500, 5, 4)$ input tensor \mathbf{X} sampled uniformly randomly from $[-1, 1]$ and scalar output $\mathbf{y} = 2\mathbf{X}[:, 0, 1] \cdot \mathbf{X}[:, 2, 3] + 3\mathbf{X}[:, 1, 0] \cdot \mathbf{X}[:, 2, 0] \cdot \mathbf{X}[:, 3, 0] + \varepsilon$. Columns 1&4: Full search; Columns 2&5: LS with $\tau = 0.5$; Columns 3&6: BB with $\delta = 0.5$.

that both LAE and LRE share the same big O complexity in terms of n . As explained in Section 2.1, we will focus on LRE since it parallels the SSE in regular regression trees.

2.3 Complexity-based Pruning

As with traditional tree-based regression methods, pruning and other forms of regularization are necessary to avoid overfitting. Adaptive pruning can be achieved based on a complexity measure $C_\alpha(T)$ following the definition in (9.16) in Hastie et al. (2009).

Revisiting the three possible splitting criteria in Section 2.1, we find that variance splitting can correspond naturally to $Q_m(T)$ in (9.16) of Hastie et al. (2009). For the low-rank splitting proposed in Algorithm 3, we propose the following modified complexity measure $C_{\text{tl}_\alpha}(T)$ which includes a low-rank induced error term $Q_{\text{tl}_m}(T)$ and is defined as:

$$C_{\text{tl}_\alpha}(T) = \sum_{m=1}^T N_m Q_{\text{tl}_m}(T) + \alpha T_l \quad (17)$$

The measure C_{tl_α} generalizes C_α by accounting for the structure and relationships in multi-dimensional data. The term $Q_{\text{tl}_m}(T)$ can be chosen as one of (3), (10) or (11) to evaluate the fitness of the leaf models given a tree structure \mathcal{T} (i.e., bias component). This captures the inherent complexity in tensor data and reflects how well the model fits the underlying tensor

structure. The variance term remains the same, representing the complexity of the tree through the number of leaves. By considering the low-rank prediction errors, the measure C_{tl_α} (as discussed in Hastie et al. (2009)) also balances the trade-off between fitting the tensor structure (the first summation term in (17) as bias) and the complexity of the decision tree (the second summation term in (17) as variance). The measure C_{tl_α} provides a way to prune the tree \mathcal{T} and maintain a simple model (high bias, low variance), which is essential for achieving good generalization performance.

In our TT models, we implement recursive pruning (without swapping or other kinds of reduction operations, for simplicity) based on whether a specific branch will reduce complexity. When we compute the first term in (17) (the second term will be affected by the choice of α) we can observe that a deeper tree may not necessarily improve the overall fit.

Pruning is needed to get a good fit and prediction in a tensor-input tree regression model. We may adjust α in the term αT_l to favor shallower trees. If we only use $\sum_{m=1}^T N_m Q_{\text{tl}_m}(T)$ in (17) to guide our pruning, the depth of the tree tensor model should be 0. We provide an example showing the effect of pruning in Appendix D.

Summary of Single Tensor Tree Model. Our efficient *tensor tree* (TT) models are constructed for scalar responses and tensor inputs with n observations and tensor dimensions d_1, d_2 . At leaf nodes we propose to fit low-rank scalar-on-tensor regression CP/Tucker models (Zhou et al., 2013; Li et al., 2018) to adapt to low-rank structures in tensors. This is a novel generalization to non-linear tree models (Chaudhuri et al., 1994; Li et al., 2000) onto non-standard tensor-input domains, and also a natural generalization of low-rank tensor models to handle heterogeneity (Figure 1).

In tensor regression trees, splitting involves entire tensor dimensions, based on low-rank approximation criteria using functions (10) to (16). Unlike traditional trees that split on single features, tensor trees assess multiple dimensions' interactions, increasing computational demands and potential overfitting. This complexity necessitates regularization through pruning and challenges interpretability due to complex decision boundaries. Low-rank approximations are computationally demanding, prompting scalability solutions in tensor settings (Kolda and Sun, 2008; Liu, 2017).

1. We propose criteria (14), (15) and (16) to split the tree structure \mathcal{T} , which reduces the dimensionality of the optimization problem $\min_{(j_0, j_1, j_2)} \mathcal{L}(j_0, j_1, j_2)$ along with randomized and branch-and-bound optimization methods (i.e., LS and BB).
2. We generalize complexity measures into (17) using new criteria for tree pruning, which achieves parsimonious partition structures.

3 Ensemble of Trees

Continuing our discussion of TT models, a single tree model tends to have large variance and overfit the data, which can produce inconsistent predictions. The idea behind tree ensemble modeling is to combine multiple models in order to improve the performance of a single TT model. Ensemble methods are foundational in modern machine learning due to their effectiveness in improving predictive performance.

In the context of tensor regressions (see Appendix E for detailed discussions), gradient boosting is particularly powerful. Each tree corrects the residuals of the previous ensemble, enabling the model to capture complex patterns in multi-dimensional data, which is crucial for tensor inputs and outputs. Gradient Boosting (GB) can also incorporate regularization, such as shrinkage and tree constraints, to prevent overfitting, which is vital when modeling high-dimensional tensor data. Boosting algorithms iteratively build decision trees, and the complexity of constructing trees grows with the dimensionality of the input space. Tensor inputs significantly increase this dimensionality, making tree construction inefficient and potentially leading to overfitting or redundant splits over the flattening space.

Algorithm 6 combines gradient boosting and adaptive sampling with the multi-dimensional prowess of tensor regression trees in order to achieve highly accurate predictive models suited especially for complex, multi-dimensional datasets. We will be able to combine m different weak learners in a residualized back-fitting scheme, and choose a learning rate (which is usually greater than $1/m$) that allows the aggregated model to leverage the prediction power.

3.1 Tensor-on-tensor: Multi-way Output Tensor Tree Ensemble

We now consider a regression problem for tensor inputs \mathbf{X}_i and tensor responses \mathbf{y}_i :

$$\mathbf{y}_i = \mathbf{g}^*(\mathbf{X}_i) + \mathbf{E}_i, i = 1, \dots, n. \quad (18)$$

for a tensor-valued function $\mathbf{g}^*: \mathbb{R}^{d_1 \times d_2} \rightarrow \mathbb{R}^{p_1 \times p_2}$ and independent mean zero noises \mathbf{E}_i . We focus on this special case but note that this approach can extend to higher order tensors.

Lock (2018) proposes to treat a *linear* tensor-on-tensor regression problem. Their methodology performs optimization directly on $\|\mathbf{y} - \mathbf{X} \circ \mathbf{B}\|_F$ with an optional regularization term penalizing the tensor rank of the coefficient tensor \mathbf{B} . To tackle the more general tensor-on-tensor problem (18), we propose two approaches for TT models based on ensemble modeling using tree regressions (Breiman et al., 1984; Breiman, 2001). In what follows, each GB ensemble will use pruning parameter $\alpha = 0.1$ and 10 single trees unless otherwise stated. We can also use other ensemble methods (e.g., random forest, Adaboost (Breiman, 1999)) or

even different kinds of ensembles for different entries (in entrywise approach) or components (in lowrank approach). (Appendix L contains simulation experiments comparing to existing random-forest methods.) As mentioned earlier, we will focus on “ensemble of GB”:

Entry-wise approach. The first approach (TTentrywise-CP, TTentrywise-Tucker) is to use a single GB ensemble to predict vector slices $\mathbf{y}[:, i, j], i = 1, \dots, p_1; j = 1, \dots, p_2$ of the tensor output as if the slices are mutually independent. This approach ignores dependence between slices, but improves computational cost since the break-down into $p_1 \times p_2$ single TT trees and the overall complexity is scaled up by a factor of $\mathcal{O}(p_1 \times p_2)$. This method is prone to overfitting, but can work well even when evaluating on testing data if the data has a large signal-to-noise ratio or if the elements of the output tensor have minimal or no correlation.

Low-rank approach. The second approach (TTlowrank-CP, TTlowrank-Tucker) is to perform CP/Tucker decomposition on the tensor output \mathbf{y} and use a single GB ensemble to predict each component (i.e., $\mathbf{a}_r, \mathbf{b}_r, \mathbf{c}_r$ in (5); $\mathbf{A}_1, \mathbf{A}_2, \mathbf{A}_3$ in (6)) in the low-rank decomposition. The low-rank decompositions align tensor structures but can be computationally intensive (the cost of decomposing \mathbf{y} can be obtained from Lemmas 1 and 2), especially when leaf nodes contain fewer samples than the selected rank of the decomposition which may not be enough to ensure a reasonable fit and generalization ability. To avoid overfitting, a general rule of thumb is to choose a higher rank for tensors with highly correlated entries in order to retain more correlation, but the optimal rank of decomposition for the tensor output is generally data-dependent. This approach allows parallelism only within each component as matrices. In addition to higher dimensionality, evaluating tensor gradients puts additional computational burden for this direct generalization. This approach allows us to break down the regressions into vector components for fitting using single trees and the overall complexity is scaled up by these factors that is dependent on the ranks we choose for CP or Tucker decompositions.

The approach *TTlowrank* offers a low-rank representation of multi-way data by leveraging the structures and relationships within tensor outputs. Decomposing the output tensor in this way enables powerful regression models that can capture complex patterns in the data. We implicitly assume the response admits a low-rank structure (which may not always be realistic) and hence perform a low-rank decomposition on the response and record weights (if CP) or core tensor (if Tucker) but fit our TT regressions on the factors. Then on a new input \mathbf{X} , we predict the corresponding factors and reconstruct the tensor output predictions using the recorded weights (if CP) or core tensor (if Tucker). Intuitively, CP decomposition preserves potential diagonality, while Tucker decomposition preserves potential orthogonality in the output tensor. This approach is suitable when the elements of the output tensor are correlated and exhibit complex relationships, and yield much smaller models compared to

the naïve approach.

3.2 Discussion on performance

Here we empirically compare the predictive performance of Lock (2018)’s approach with that of our two TT approaches. To generate our datasets, we sample entries of \mathbf{X} from a uniform distribution on $[0, 1]$ and compute \mathbf{y} using functions listed in the table in Appendix M (whose ranges are all within $[-1, 2]$), and add a uniform noise of scale 0.01. Training and testing sets are generated independently. For rrr methods (Lock, 2018), we set the R rank parameter and leave the remaining parameters as the package default. For TT methods, we set both splitting ranks and regression ranks to be the same as R, with `max_depth = 3` and pruning measures $\alpha = 0.01$. We use a GB ensemble with 10 estimators and learning rate 0.1 uniformly.

The table in Appendix M shows the out-of-sample errors of each model, where we see that at least one of the TT methods either ties or outperforms both rrr methods in 23 of the 24 tested scenarios. The comparison can be separated into two groups. One group (Linear/Non-linear) explores the power of using GB ensemble TT models (with pruning) along with the two approaches for tensor-on-tensor regression tasks (here for simplicity we choose the same regression rank R for CP models or (R, R, R) for Tucker models for both input \mathbf{X} and output \mathbf{y}). Using the RPE metric, we can observe that TT with GB for tensor output performs quite competitively with the rrr models and improves as the low-rank models’ rank increases, and only TT model can possibly capture non-linear interactions as expected, since higher rank means better approximation to the \mathbf{y} . In the TTlowrank method with Tucker decomposition on \mathbf{y} , the Tucker decomposition is behaving very badly regardless of ranks and shows non-convergence after maximal iterations are reached, since the components in \mathbf{y} possess high correlations. This partially explains why its RPE is greater than 1 for the linear and non-linear examples, and its performance is the worst for this group due to the fact that we do not assume low-rank structure in the output \mathbf{y} . It seems that the practice of using rank (R, R, R) for Tucker decomposition on \mathbf{y} does not reflect the tensor structure in the output well in this group of experiments. In both linear and non-linear scenarios, the lowest RPE values are often seen with rrrBayes and TTlowrank_Cp methods, which closely align with rrr methods. This indicates that tree-based tensor regression methods improve in efficiency as rank increases due to better approximation quality.

The second set of experiments (Exact CP/Exact Tucker) explores scenarios with significant TT trees and pruning in GB ensembles. By setting `max_depth>0`, localized effects on data from tree partitioning help capture periodic behaviors in learners. Both TTentrywise

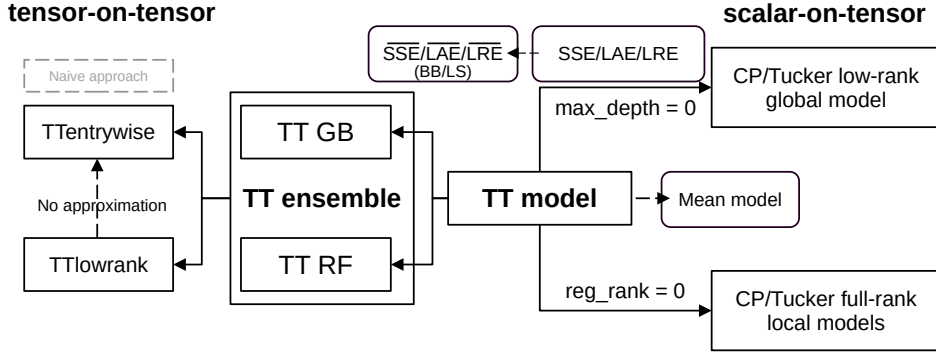


Figure 3: Design of the TT models (scalar-on-tensor) and ensembles (tensor-on-tensor).

and TTlowrank methods perform well under CP decomposition, showing competitive performance against rrr models. However, Tucker decomposition can experience non-convergence issues at (R, R, R) ranks, identified by `tensorly`, necessitating re-runs to confirm convergence. In these cases, signals depend solely on low-rank \mathbf{X} , benefiting TT models with appropriate ranks R . In practice, the mode-specific ranks can be different like (R_1, R_2, R_3) for better flexibility; and the model-specific ranks can also vary for different leaf nodes to account for possible heterogeneity.

Summary of Tensor Tree Ensembles Boosting methods like GB employ functional gradient descent to minimize a specified loss function. The process involves calculating pseudo-residuals, fitting new trees to these residuals, and updating the model iteratively.

To address multi-way regression problems by performing optimization directly on tensor outputs, we deploy a GB ensemble of TT along with two alternative approaches — entry-wise and low-rank — for tensor regression trees (TT models) using ensemble methods.

Figure 3 illustrates how we construct ensemble models and how GB (or RF) ensemble of TT models can be utilized to perform tensor-on-tensor regressions. We adopt boosting for tensor output regressions for their ability to sequentially improve models by focusing on residuals, making them suitable for complex tensor-on-tensor regression tasks.

4 Theoretical Guarantees

Although this paper focuses on developing new modeling methodologies and fast training algorithms, we use existing theoretical results to support the validity of our modeling designs. The results in this section all assume scalar responses.

4.1 Coefficient Asymptotics

A fixed tree of depth K has at most 2^K leaf nodes. In the recursive partition literature (e.g., (2.27) in Gordon and Olshen (1978)), it is commonly assumed that for each leaf node t , the number of samples n_t tends to infinity when the overall sample size n tends to infinity. This condition obviously holds when we split on the median in the vector-input case, but is not necessarily true if we split according to (8) or (13). Under this assumption, within each leaf node we can directly apply existing coefficient estimate consistency results for CP and Tucker regression models (Zhou et al., 2013; Li et al., 2018).

Proposition 2. *For a fixed complete binary tree of depth $K < \infty$, assume for each leaf node t that the number of i.i.d. samples $n_t \rightarrow \infty$ and the leaf model parameter space is compact.*

(a) (Theorem 1 in Section 4.3 of Zhou et al. (2013)) *For the leaf node CP model with mean-zero normal error and $\mathbf{X}[i,:,:] \in R_t$, suppose the true coefficient $\mathbf{B}_0(t) = \sum_{r=1}^R \lambda_r(t) \mathbf{a}_r(t) \times \mathbf{b}_r(t) \times \mathbf{c}_r(t)$ of node t is identifiable up to permutation in the sense of Proposition 4 in Zhou et al. (2013). Then the MLE $\hat{\mathbf{B}}_n(t)$ converges to $\mathbf{B}_0(t)$ in probability.*

(b) (Theorem 1 in Section 4.3 of Li et al. (2018)) *For the leaf node Tucker model with mean-zero normal error and $\mathbf{X}[i,:,:] \in R_t$, suppose the true coefficient $\mathbf{B}_0(t) = \mathbf{G}(t) \times_1 \mathbf{A}_1(t) \times_2 \mathbf{A}_2(t) \times_3 \mathbf{A}_3(t)$ of node t is identifiable up to permutation in the sense of Proposition 3 in Li et al. (2018). Then the MLE $\hat{\mathbf{B}}_n(t)$ converges to $\mathbf{B}_0(t)$ in probability.*

Though often presupposed, the condition $n_t \rightarrow \infty$ assumes fixed tree and leaf node partitions R_t , which is unrealistic since typically the partition changes as $n \rightarrow \infty$. It also requires an additive true function $f(\mathbf{X}) = \sum_{t \text{ is a leaf node}} \mathbf{X} \circ \mathbf{B}_0(t) \cdot \mathbf{1}(\mathbf{X} \in R_t)$ whose summands are piece-wise multilinear functions. Also, even under these restrictions we still do not have estimates for the ranks of tensor coefficients, as pointed out by Zhou et al. (2013) and Li et al. (2018). However, Proposition 2 confirms one important aspect that if $f(\mathbf{X}) = \mathbf{X} \circ \mathbf{B}_0$ for some global \mathbf{B}_0 (for CP or Tucker model), our tree model produces consistent coefficient estimates for *arbitrary* (hence dynamic) partitions, since $\mathbf{B}_0 = \mathbf{B}_0(t)$ and

$$\mathbf{X} \circ \mathbf{B}_0 = \mathbf{X} \circ \mathbf{B}_0 \cdot \sum_{t \text{ is a leaf node}} \mathbf{1}(\mathbf{X} \in R_t) = \sum_{t \text{ is a leaf node}} \mathbf{X} \circ \mathbf{B}_0 \cdot \mathbf{1}(\mathbf{X} \in R_t). \quad (19)$$

With this positive result, our tensor tree model for any maximum depth K is no worse than the standalone CP or Tucker model in terms of consistency under $f(\mathbf{X}) = \mathbf{X} \circ \mathbf{B}_0$.

4.2 Oracle Error Bounds for (9)

As seen above, the fitted mean function from a decision tree regression model lies in the additive class with iterative summation across tensor dimensions d_1, d_2 :

$$\mathcal{G}^1 := \left\{ g: \mathbb{R}^{d_1 \times d_2} \rightarrow \mathbb{R} \mid g(\mathbf{X}) = \sum_{i_2=1}^{d_2} \sum_{i_1=1}^{d_1} g_{i_1, i_2}(\mathbf{X}[i_1, i_2]) \right\}, \quad (20)$$

which is essentially the same functional class as that in Klusowski and Tian (2024) but with both dimensions additively separable. Within this class, a more useful result regarding the prediction risk can be established.

Theorem 3. *(Empirical bounds for TT) Suppose data $\mathbf{X}^{(n)} \in \mathbb{R}^{n \times d_1 \times d_2}$ and $\mathbf{y} \in \mathbb{R}^{n \times 1}$ are generated by model (7) where g^* is not necessarily in \mathcal{G}^1 . Let g_K be the regression function of a TT model split by minimizing (9) with maximal depth K and fitting mean models at the leaves. Then the empirical risk $\hat{\mathcal{R}}(g) = n^{-1} \sum_{i=1}^n (y_i - g(\mathbf{X}^{(n)}[i, :, :]))^2$ has the bound:*

$$\hat{\mathcal{R}}(g_K) \leq \inf_{g \in \mathcal{G}^1} \left\{ \hat{\mathcal{R}}(g) + \frac{\|g\|_{TV}^2}{K+3} \right\}$$

where $\|g\|_{TV}$ is (the infimum over all additive representations of $g \in \mathcal{G}^1$ of) the aggregated total variation of the individual component functions of g .

Proof. See Appendix H. □

Using the same argument as in Theorem 4.3 in Klusowski and Tian (2024), the following theorem bounds the expected L_2 error between the true signal g^* (not necessarily in \mathcal{G}^1) and the mean function g_K of a complete tree of depth $K \geq 1$ constructed by minimizing (9).

Theorem 4. *(Oracle inequalities for TT) Suppose data $\mathbf{X}^{(n)} \in \mathbb{R}^{n \times d_1 \times d_2}$ and $\mathbf{y} \in \mathbb{R}^{n \times 1}$ are generated by the model $y = g^*(\mathbf{X}) + \varepsilon$ for additive sub-Gaussian noise ε (i.e., $\mathbb{P}(\varepsilon \geq u) \leq 2 \exp(-u^2/2\sigma^2)$ for some $\sigma^2 > 0$). Let g_K be the regression function of a TT model split by minimizing (9) with maximal depth K and fitting mean models at the leaves. Then*

$$\mathbb{E}(\|g^* - g_K\|^2) \leq 2 \inf_{g \in \mathcal{G}^1} \left\{ \|g^* - g\|^2 + \frac{\|g\|_{TV}^2}{K+3} + C_1 \cdot \frac{2^K \log^2(n) \log(nd_1 d_2)}{n} \right\}$$

where C_1 is a positive constant depending only on $\|g^*\|_\infty$ and σ^2 .

This result does not cover CP or Tucker regressions at the leaf nodes. Also, if the tree is split using the LAE criterion (10), then the correlation-based expansion in Klusowski

and Tian (2024) will no longer work. It remains an open question whether the LAE-based Algorithm 3 is consistent even when $K = 1$.

5 Data Experiments

5.1 Effect of Different Splitting Criteria

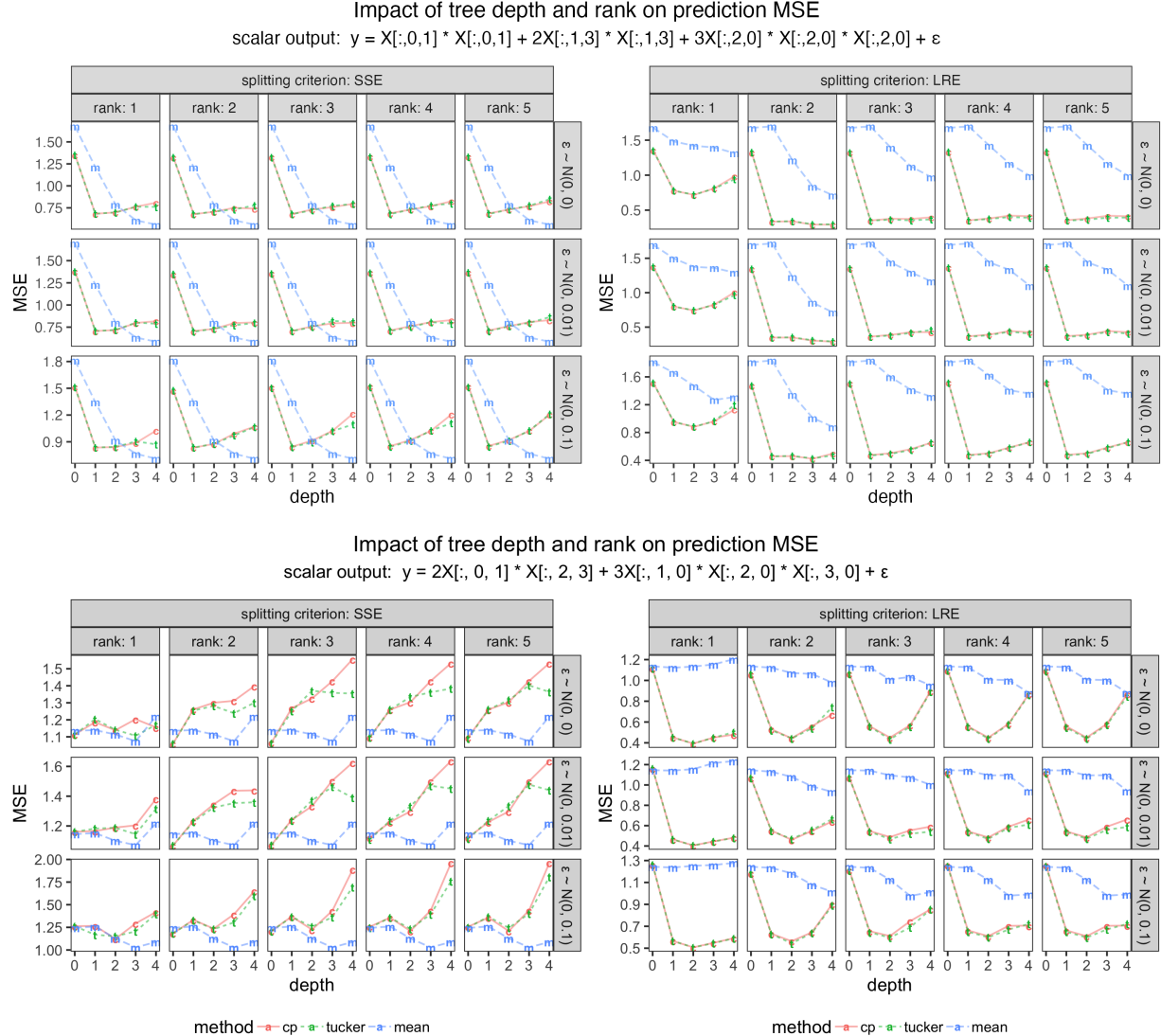


Figure 4: Out-of-sample MSE comparison of CP, Tucker ($\tau = 1$), and mean predictions for tree models of different max_depth and split by either the SSE (9) or LRE (11), we use the same splitting and fitting ranks. We sample a $(1000, 5, 4)$ input tensor uniformly from $[-1, 1]$. MSEs are averaged over 10 seeds.

Splitting criteria allow tree-based regression models to capture interactions between the predictors that would not be captured by a standard regression model (Hastie et al., 2009; Klusowski, 2020). This approach can also be generalized to tensors of any order. Conditioned on the splitted partitions, we may take the sample mean as predictive values, or fit a regression model (e.g., linear or tensor regression) to the data on each partition.

The standard setting of our model is to let the `split_rank` parameter to be the same as `CP_reg_rank` (or `Tucker_reg_rank`, see Table 3 for detailed parameter specification). In most of the applications considered in this paper, we set `split_rank` to be the same as the rank chosen for the leaf node regressions. This practice reflects our belief that the model and recursive partition regime share the same low-rank structure assumption. However, it is possible to choose split and regression ranks to be different and even adaptively when the low-rank structure within each group or as the tree grows deeper.

Selecting splitting criteria. We examine the MSE in Figure 4¹. When split using the SSE criterion (9), the tensor models perform comparably with the mean model, with neither consistently outperforming the other. The underlying mechanisms that split the data according to the variation of \mathbf{y} do not necessarily capture the tensor structure better.

In contrast, when split using the LRE criterion (11), the tensor models perform better than the mean models. Hence the remainder of the subsection highlights the enhanced performance of tensor models when utilizing the LRE criterion. Interestingly, the MSE of the CP/Tucker models does not monotonically decrease as decomposition rank and tree depth increase. In Figure 4, the MSEs at rank 1 are different from the MSEs at ranks 2,3,4,5. Rank also seems to affect MSEs at larger tree depths. Otherwise, rank seems to not make much difference in these two examples. Regarding depth, the top half of Figure 4 shows that with an appropriate rank (i.e., ranks 2,3,4,5), our tree-based low-rank model exhibit an L-shaped MSE pattern with respect to depth can outperform the mean model for any of the tested tree depths. However, in the bottom half of Figure 4, the CP/Tucker models exhibit a U-shaped MSE pattern with respect to depth and may perform worse than a mean model if the tree depth is not appropriately selected.

Interaction in signals. The tensor model is quite good at capturing the non-separable interactions like $\mathbf{X}[:, 1, 3] * \mathbf{X}[:, 1, 3]$ and $\mathbf{X}[:, 1, 0] * \mathbf{X}[:, 2, 0] * \mathbf{X}[:, 3, 0]$ in the tensor input. In Figure 4, where triplet interactions $\mathbf{X}[:, 2, 0] * \mathbf{X}[:, 2, 0] * \mathbf{X}[:, 2, 0]$ or $\mathbf{X}[:, 1, 0] * \mathbf{X}[:, 2, 0] * \mathbf{X}[:, 3, 0]$ exist, the 3-way tensor decomposition helps to fit a low-rank regression model to outperform the usual mean model used along with tree regressions.

¹In the SSE experiment with rank 2 and $N(0, 0.1)$ noise, we found 4 out of 10 cases raising possible non-convergence warnings from `tensorly`, for other experiments there are 1 or 2.

On one hand, increasing the regression ranks² will have a saturation effect, where the performance may not change after a certain rank threshold. This is clear in both LAE and LRE columns. The difference is that increasing LAE may deteriorate the performance (Figure 4) while LRE cannot deteriorate the performance, since it is purely splitting based on reducing the tensor regression ranks of the chosen leaf models.

On the other hand, the tree depth (max_depth) will not have this saturation effect. We can observe that there is usually a 'sweetspot' depth (e.g., depth 1,2,3 in the bottom half of Figure 4). If we keep increasing the tree depth, we will enter the second half of the U-shape and deteriorate the tree-based tensor-model. As shown by Figure 4, the low-rank CP regression models at leaf nodes improve prediction MSE compared to the traditional mean predictions but depends on the depth.

5.2 Comparison with Other Tensor Models

The Tensor Gaussian Process (TensorGP, Yu et al. (2018)) extends Gaussian Processes (GPs, Luo et al. (2022)) to high-dimensional tensor data using a multi-linear kernel with a low-rank approximation. In regular GPs, the covariance matrix \mathbf{K} is derived from a kernel function $k(\mathbf{X}, \mathbf{X}')$ which typically depends on the Euclidean distance between points \mathbf{X}, \mathbf{X}' . For n data points, the matrix \mathbf{K} has size $n \times n$ with elements $\mathbf{K}_{ij} = k(\mathbf{X}[i, :], \mathbf{X}[j, :])$.

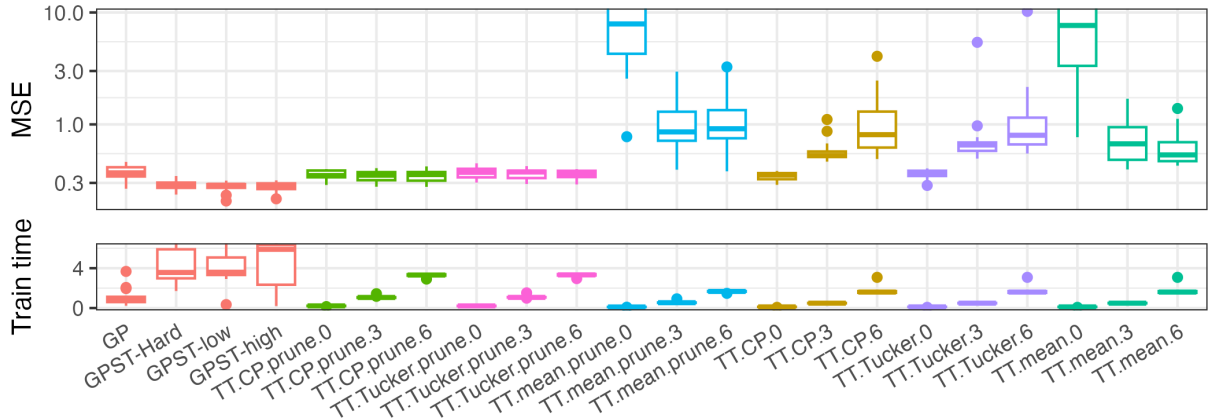


Figure 5: Out-of-sample MSE and training time (minutes) of our tensor-input tree (TT), tensor-GP, GPST, CP (ranks = 3), and Tucker (ranks = [3,3,3]). All models are fitted (with 75% training set of size 1000 4-dimensional tensor) on 20 batches of the synthetic datasets in Table 1 of Sun et al. (2023). The final character of each TT method label indicates the method's set maximum depth. Our TT model is split using SSE criterion (9). For the TT_prune methods, the tree is pruned with $\alpha = 0.1$ in (17).

²We choose the split_rank and CP_reg_rank/Tucker_reg_rank to be the same as our default.

Our TT method is significantly faster than the $\mathcal{O}(n^3)$ complexity of GP models, making it feasible for high-dimensional data. The TensorGP model optimization seeks optimal low-rank matrices to preserve data structures using a covariance kernel in tensor form. Similarly, the Tensor-GPST model (Sun et al., 2023), uses tensor contraction for dimension reduction, akin to pre-PCA in standard GP models. This includes anisotropic total variation regularization for generating sparse, smooth latent tensors.

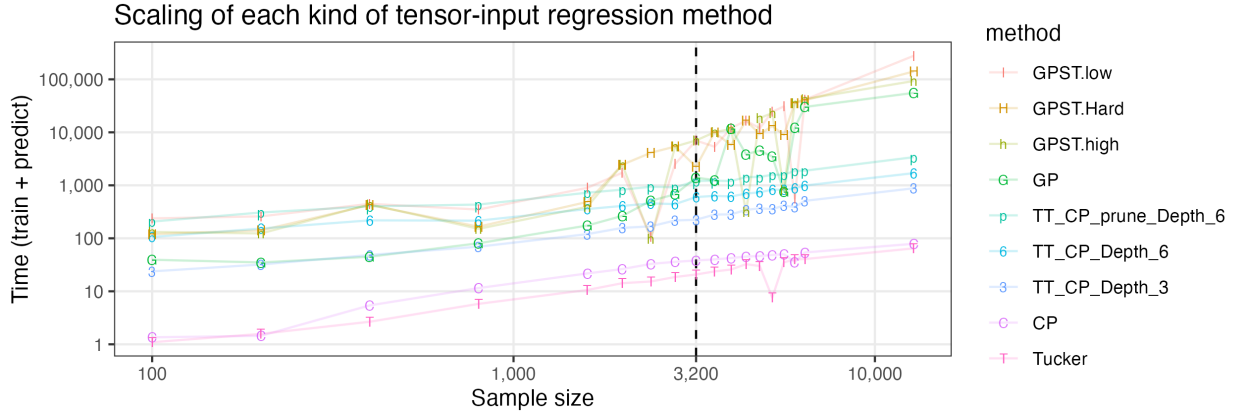


Figure 6: In-sample and out-of-sample training time (seconds) against the sample size for the experiments in Figure 5. For TT models with pruning, we experiment with $\text{max_depth}=3,6$ and select $\alpha = 0.5$ in (17) and perform only one fit on an Intel i9-10885H 2.40GHz machine.

Figures 5 and 6 in the main text and Figure 8 in Appendix J compare model performances and training times using Sun et al. (2023)'s synthetic data. GPST models excel in testing MSE, outperforming tensor-GP models in fitting and generalization. However, TT models show lower training but higher testing MSE, indicating overfitting; pruning improves CP/Tucker leaf models' MSE, making them nearly comparable to GPST but with less depth pruning compared to mean models. Although GPST has longer training and prediction times, unpruned TT models are faster, with even pruned versions having lower computational times than tensor GP models, as shown by Proposition 1. With pruning, our TT models take longer to compute, but all TT models with depth ≤ 3 are still much faster to compute than the tensor GP models, echoing our Proposition 1.

5.3 More Applications

EEG Data Our first example uses the EEG dataset from in the **TRES** R package (Zeng et al., 2021). We use $61 \times 64 \times 64$ tensor inputs of $n = 61, d_1 = d_2 = 64$ parsed from EEG dataset and a binary label \mathbf{y} . Using TRR (\mathbf{y} as vector predictor) and TPR (\mathbf{X} as tensor predictor) from this package, we illustrate the fitted coefficients from TRS models

with different fitting methods (i.e., 1D/FG/OLS/PLS).

Analogous to Figure 1, the fourth and fifth rows in the figure in Appendix N each consist of eight panels; each panel represents a 64×64 coefficient corresponding to a low-rank CP or Tucker model at leaf nodes, which are based on a subset (induced by low-rank splitted trees with target rank $R = 5$) along the first mode of the input tensor \mathbf{X} . The eight panels in the fourth and fifth rows appear to overlap and collectively approximate the first two panels (1D and FG coefficients) in the first (TRES.TRR) and second (TRES.TPR) rows. This can be attributed to several factors. One is the redundancy in the subsets along the first dimension; if these subsets either overlap significantly or are highly correlated, the resulting reconstructions in each panel would naturally appear similar, otherwise dis-similar. We find that the TT coefficients with sufficient depth are more similar to the TPR coefficients, seeing as both models take tensors as inputs, than they are to the TRR coefficients, where TRR takes tensors as the response. In particular, the 3,5,6-th leaf node models' coefficients seem to capture the TRES.TPR (1D, FG, PLS) coefficient patterns. Another explanation could be the complementarity of the features captured in each panel. If each panel captures unique but complementary structural or informational elements of the original tensor, their collective representation would naturally approximate the entire tensor effectively; this may explain why the deeper layer models seem like a decomposition of the depth 0 model. Lastly, the inherent nature of CP and Tucker decomposition as a low-rank approximation implies that even a subset of the first dimension's factor vectors, when integrated with the corresponding vectors from other modes, can capture significant global features of the original tensor \mathbf{X} .

Facial Image Our second example uses frontalized facial images as in Lock (2018) showing forward-facing faces achieved by rotating, scaling, and cropping original images. The highly aligned images facilitate appearance comparisons. Each image has 90×90 pixels, with each pixel containing red, green, and blue channel intensities. We randomly sample 500 images, so the predictor tensor \mathbf{X} has dimensions $500 \times 90 \times 90 \times 3$, and the response tensor \mathbf{Y} has dimensions 500×72 . We center each image tensor by subtracting the mean of all image tensors. Another randomly sampled 500 images and response are used as a validation set.

Lock (2018) found the rrr method with $\lambda = 10^5$ achieved an RPE of 0.568, ranging from 0.5 to 0.9, but fairly comparing regularizations is complex. At each leaf t , introducing a unique regularization term $\lambda(t)$ is challenging due to varying sample sizes across leaf nodes. Hence, all models in our study use no regularization ($\lambda_{TT} = 0$), simplifying comparisons. TTentrywise and TTlowrank perform reasonably (see Table 1), but they do not match the tensor-on-tensor rrr and Bayesian rrrBayes models (Lock, 2018). TT offers an alternative for tensor-on-tensor regression without complex prior specifications or MCMC computations

		TTentrywise_CP	TTentrywise_Tucker	TTlowrank_CP		TTlowrank_Tucker	
rank		RMSE	RPE	RMSE	RPE	RMSE	RPE
3		9.0007	0.7083	9.0218	0.7150	8.8316	0.6566
5		9.0523	0.7247	9.0729	0.7313	8.8761	0.6699
15		9.0582	0.7266	9.1162	0.7454	8.9741	0.7000
						10.5614	1.3447

Table 1: RMSE and RPE from TT models trained on a resampled Facial Image dataset (Lock, 2018) with CP/Tucker methods and TTentrywise/TTlowrank approaches.

(Gahrooei et al., 2021; Luo and Zhang, 2022; Wang and Xu, 2024), but managing the high-dimensional input and computational demands for 720 different tree models in TTentrywise, each requiring intricate splitting and pruning, remains a significant challenge.

6 Conclusion

Our paper contributes to scalar-on-tensor and tensor-on-tensor regressions using tree-based models (Algorithm 1), especially designed for high-dimensional tensor data. Unlike traditional regression trees which handle vector inputs, our models are tailored for multi-way array inputs, significantly enhancing their utility for complex data types.

We developed both randomized and deterministic algorithms to efficiently fit these models (Algorithm 3 and 4), crucial due to the high computational demand of tensor operations. These models perform competitively against established tensor-input Gaussian Process models (Sun et al., 2023; Yu et al., 2018) and are computationally more efficient, utilizing techniques like leverage score sampling and branch-and-bound optimization.

There are other types of tensor products, such as the Khatri-Rao products, which offer granular feature spaces and more detailed splitting rules (Section 2.1) analogous to the oblique trees (Murthy et al., 1994; Breiman et al., 1984). Additionally, kernel-based approaches are well-suited for capturing complex, non-linear relationships and could enhance the predictive power for mixed inputs (Luo et al., 2024). However, tensor product inequalities are not necessarily computationally tractable, and efficient formats like tensor-train are needed for practical implementations (Oseledets, 2011).

Further, we expand our methods to tensor-on-tensor regressions through tree ensembles, addressing a gap in existing non-parametric models that can process both tensor inputs and outputs. This includes implementing new tensor-specific splitting criteria like variance splitting and low-rank approximation, and exploring potential applications such as tensor

compression (Kielstra et al., 2024).

While we demonstrate the effectiveness of these models and their ensembling methods, theoretical aspects like the consistency of dynamic trees and error bounds for ensemble tensor models remain open for further research. Our tree-based method could be extended to be robust to rotations(van der Wilk et al., 2018) via rotation forests (Rodriguez et al., 2006), which remains to be explored in tensor data setting. Our work paves the way for future studies to explore these areas within the framework of complex data analysis.

Acknowledgment

HL thanks LBNL for providing computational resources in pilot experiments. HL was supported by U.S. Department of Energy under Contract DE-AC02-05CH11231 and U.S. National Science Foundation NSF-DMS 2412403. LM and AH were partly supported by NSF grants DMS-1749789 and NIGMS grant R01-GM135440. LM was also partly supported by NSF grant DMS-2152999.

We thank the anonymous referees and the Associate Editor for their constructive feedback.

References

Amit, Y. and D. Geman (1997). Shape quantization and recognition with randomized trees. *Neural computation* 9(7), 1545–1588.

Athey, S., J. Tibshirani, and S. Wager (2019). Generalized random forests.

Bi, X., X. Tang, Y. Yuan, Y. Zhang, and A. Qu (2021). Tensors in statistics. *Annual review of statistics and its application* 8, 345–368.

Breiman, L. (1999). Prediction games and arcing algorithms. *Neural computation* 11(7), 1493–1517.

Breiman, L. (2001). Random forests. *Machine Learning* 45, 5–32.

Breiman, L. et al. (1984). Classification and regression trees.

Bulté, M. and H. Sørensen (2024). Medoid splits for efficient random forests in metric spaces. *Computational Statistics & Data Analysis*, 107995.

Capitaine, L., J. Bigot, R. Thiébaut, and R. Genuer (2024). Fréchet random forests for metric space valued regression with non euclidean predictors. *Journal of Machine Learning Research* 25(355), 1–41.

Chaudhuri, P., M.-C. Huang, W.-Y. Loh, and R. Yao (1994). Piecewise-polynomial regression trees. *Statistica Sinica*, 143–167.

Chen, T. and C. Guestrin (2016). Xgboost: A scalable tree boosting system. In *Proceedings of the 22Nd ACM SIGKDD International Conference on Knowledge Discovery and Data Mining*, KDD '16, New York, NY, USA, pp. 785–794. ACM.

Chickering, D. M., C. Meek, and R. Rounthwaite (2001). Efficient determination of dynamic split points in a decision tree. In *Proceedings 2001 IEEE international conference on data mining*, pp. 91–98. IEEE.

Chipman, H., E. I. George, and R. E. McCulloch (1998). Bayesian cart model search. *Journal of the American Statistical Association* 93(443), 935–948.

Chipman, H., P. Ranjan, and W. Wang (2012). Sequential design for computer experiments with a flexible Bayesian additive model. *Canadian Journal of Statistics* 40(4), 663–678.

Chipman, H. A., E. I. George, and R. E. McCulloch (2010). Bart: Bayesian additive regression trees. *The Annals of Applied Statistics* 4(1), 266–298.

Denison, D., A. Smith, and B. Mallick (1998). Bayesian cart model search: Comment. *Journal of the American Statistical Association* 93(443), 954–957.

Freund, Y. and R. E. Schapire (1997). A decision-theoretic generalization of on-line learning and an application to boosting. *Journal of computer and system sciences* 55, 119–139.

Friedman, J., T. Hastie, S. Rosset, R. Tibshirani, and J. Zhu (2004). Discussion of boosting papers. *Annual Statistics* 32, 102–107.

Friedman, J. H. (2001). Greedy function approximation: A gradient boosting machine. *The Annals of Statistics* 19, 1189–1232.

Gahrooei, M. R., H. Yan, K. Paynabar, and J. Shi (2021). Multiple tensor-on-tensor regression: An approach for modeling processes with heterogeneous sources of data. *Technometrics* 63(2), 147–159.

Geurts, P., D. Ernst, and L. Wehenkel (2006). Extremely randomized trees. *Machine learning* 63, 3–42.

Gordon, L. and R. A. Olshen (1978). Asymptotically efficient solutions to the classification problem. *The Annals of Statistics*, 515–533.

Guhaniyogi, R., S. Qamar, and D. B. Dunson (2017). Bayesian tensor regression. *Journal of Machine Learning Research* 18(79), 1–31.

Guo, W., I. Kotsia, and I. Patras (2011). Tensor learning for regression. *IEEE Transactions on Image Processing* 21(2), 816–827.

Hastie, T., R. Tibshirani, J. H. Friedman, and J. H. Friedman (2009). *The elements of statistical learning: data mining, inference, and prediction*, Volume 2. Springer.

Johndrow, J. E., A. Bhattacharya, and D. B. Dunson (2017). Tensor decompositions and sparse log-linear models. *Annals of statistics* 45(1), 1.

Kielstra, P. M., T. Shi, H. Luo, J. Qian, and Y. Liu (2024+). A linear-complexity tensor butterfly algorithm for compressing high-dimensional oscillatory integral operators. *ongoing*, 1–39.

Klusowski, J. (2020). Sparse learning with cart. *Advances in Neural Information Processing Systems 33*, 11612–11622.

Klusowski, J. M. and P. M. Tian (2024). Large scale prediction with decision trees. *Journal of the American Statistical Association 119*(545), 525–537.

Kolda, T. G. and B. W. Bader (2009). Tensor decompositions and applications. *SIAM review 51*(3), 455–500.

Kolda, T. G. and J. Sun (2008). Scalable tensor decompositions for multi-aspect data mining. In *2008 Eighth IEEE international conference on data mining*, pp. 363–372. IEEE.

Kossaifi, J., Y. Panagakis, A. Anandkumar, and M. Pantic (2019). Tensorly: Tensor learning in python. *Journal of Machine Learning Research 20*(26), 1–6.

Krawczyk, B. (2021). Tensor decision trees for continual learning from drifting data streams. *Machine Learning 110*(11-12), 3015–3035.

Lawler, E. L. and D. E. Wood (1966). Branch-and-bound methods: A survey. *Operations research 14*(4), 699–719.

Li, K.-C., H.-H. Lue, and C.-H. Chen (2000). Interactive tree-structured regression via principal hessian directions. *Journal of the American Statistical Association 95*(450), 547–560.

Li, L. and X. Zhang (2017). Parsimonious tensor response regression. *Journal of the American Statistical Association 112*(519), 1131–1146.

Li, X., D. Xu, H. Zhou, and L. Li (2018). Tucker tensor regression and neuroimaging analysis. *Statistics in Biosciences 10*, 520–545.

Liu, Y. (2017). Low-rank tensor regression: Scalability and applications. In *2017 IEEE 7th International Workshop on Computational Advances in Multi-Sensor Adaptive Processing (CAMSAP)*, pp. 1–5. IEEE.

Lock, E. F. (2018). Tensor-on-tensor regression. *Journal of Computational and Graphical Statistics 27*(3), 638–647.

Luo, H., Y. Cho, J. W. Demmel, X. Li, and Y. Liu (2024). Hybrid Parameter Search and Dynamic Model Selection for Mixed-Variable Bayesian Optimization. *Journal of Computational and Graphical Statistics 0*(0), 1–14.

Luo, H. and A. Ma (2025). Tensor randomized frontal sketching method to large-scale linear systems. *Numerical Mathematics: Theory, Methods and Applications*, 1–30, to appear.

Luo, H., G. Nattino, and M. T. Pratola (2022). Sparse Additive Gaussian Process Regression. *Journal of Machine Learning Research* 23(61), 1–34.

Luo, H. and M. T. Pratola (2022). Sharded Bayesian Additive Regression Trees. *arXiv:2306.00361*, 1–46.

Luo, Y. and A. R. Zhang (2022). Tensor-on-tensor regression: Riemannian optimization, over-parameterization, statistical-computational gap, and their interplay. *arXiv preprint arXiv:2206.08756*.

Malik, O. A. and S. Becker (2018). Low-rank tucker decomposition of large tensors using tensorsketch. *Advances in neural information processing systems* 31.

Mentch, L. and S. Zhou (2020). Randomization as regularization: A degrees of freedom explanation for random forest success. *The Journal of Machine Learning Research* 21(1), 6918–6953.

Minster, R., I. Viviano, X. Liu, and G. Ballard (2023). Cp decomposition for tensors via alternating least squares with qr decomposition. *Numerical Linear Algebra with Applications* 30(6), e2511.

Morrison, D. R., S. H. Jacobson, J. J. Sauppe, and E. C. Sewell (2016). Branch-and-bound algorithms: A survey of recent advances in searching, branching, and pruning. *Discrete Optimization* 19, 79–102.

Murray, R., J. Demmel, M. W. Mahoney, N. B. Erichson, M. Melnichenko, O. A. Malik, L. Grigori, M. a. M. E. L. Dereziński, T. Liang, H. Luo, and J. J. Dongarra (2023). Randomized numerical linear algebra: A perspective on the field with an eye to software. *arXiv preprint arXiv:2302.11474*.

Murthy, S. K., S. Kasif, and S. Salzberg (1994). A system for induction of oblique decision trees. *Journal of artificial intelligence research* 2, 1–32.

Oh, S., N. Park, S. Lee, and U. Kang (2018). Scalable tucker factorization for sparse tensors-algorithms and discoveries. In *2018 IEEE 34th International Conference on Data Engineering (ICDE)*, pp. 1120–1131. IEEE.

Oseledets, I. V. (2011). Tensor-train decomposition. *SIAM Journal on Scientific Computing* 33(5), 2295–2317.

Papadogeorgou, G., Z. Zhang, and D. B. Dunson (2021). Soft tensor regression. *Journal of Machine Learning Research* 22(219), 1–53.

Pratola, M. T. (2016). Efficient metropolis-hastings proposal mechanisms for bayesian regression tree models. *Bayesian Analysis* 11, 885–911.

Pratola, M. T., H. A. Chipman, J. R. Gattiker, D. M. Higdon, R. McCulloch, and W. N. Rust (2014). Parallel Bayesian additive regression trees. *Journal of Computational and Graphical Statistics* 23, 830–852.

Prokhorenkova, L., G. Gusev, A. Vorobev, A. V. Dorogush, and A. Gulin (2018). Catboost: unbiased boosting with categorical features. *Advances in neural information processing systems 31*.

Qiu, R., Z. Yu, and R. Zhu (2024). Random forest weighted local fréchet regression with random objects. *Journal of Machine Learning Research 25*(107), 1–69.

Rodriguez, J. J., L. I. Kuncheva, and C. J. Alonso (2006). Rotation forest: A new classifier ensemble method. *IEEE transactions on pattern analysis and machine intelligence 28*(10), 1619–1630.

Sun, H., W. Manchester, M. Jin, Y. Liu, and Y. Chen (2023, 23–29 Jul). Tensor Gaussian process with contraction for multi-channel imaging analysis. *202*, 32913–32935.

van der Wilk, M., M. Bauer, S. John, and J. Hensman (2018). Learning invariances using the marginal likelihood. *Advances in Neural Information Processing Systems 31*.

Wang, K. and Y. Xu (2024). Bayesian tensor-on-tensor regression with efficient computation. *Statistics and its interface 17*(2), 199.

Yu, R., G. Li, and Y. Liu (2018). Tensor regression meets gaussian processes. In *International Conference on Artificial Intelligence and Statistics*, pp. 482–490. PMLR.

Zeng, J., W. Wang, and X. Zhang (2021). Tres: An r package for tensor regression and envelope algorithms. *Journal of Statistical Software 99*, 1–31.

Zhou, H., L. Li, and H. Zhu (2013). Tensor regression with applications in neuroimaging data analysis. *Journal of the American Statistical Association 108*(502), 540–552.

SUPPLEMENTARY MATERIAL

A Performance Metrics

The performance of a tensor-input predictive model $\hat{\mathbf{y}}$ can be quantified using the classical regression metric Mean Square Error (MSE) $\|\mathbf{y} - \hat{\mathbf{y}}\|_2^2$ (or root MSE). We also consider the Relative Prediction Error (RPE) (Lock, 2018) defined as $\text{RPE} = \|\mathbf{y} - \hat{\mathbf{y}}\|_F^2 / \|\mathbf{y}\|_F^2$ on testing data (a.k.a. SMSPE (Gahrooei et al., 2021)), where $\|\cdot\|_F$ denotes the Frobenius norm on the vectorized form of a tensor. Unlike MSE, RPE is a *normalized* discrepancy between the predicted and actual values. To supplement these prediction error metrics, we also provide complexity analysis with actual time benchmarks. Many existing tensor models (Sun et al., 2023) including the low-rank models (Liu, 2017) have been shown to be bottlenecked by scalability, and our tree models and ensemble variant provide a natural divide-and-conquer approach addressing this.

B Methods of efficient search for splitting coordinates.

Existing efficient methods (Luo and Pratola, 2022; Chickering et al., 2001) for splitting point optimization (i.e., search among possible points for the above loss functions) usually rely on the distribution assumptions on the candidates. In our case, this assumption is usually not realistic due to the complex correlation between dimensions of the input tensor. To reduce the $N^* \cdot (\max_i d_i)^K$ factor further, we propose two methods for shrinking the search space of these optimization problems in order to quickly solve the minimization problems for (10) or (11). Both methods have existed in the optimization community for a while and exhibit trade-offs between efficiency and accuracy, but to our best knowledge are applied in regression trees for the first time.

Model \ Item	Decision Trees	Extra-Trees (ERT)	Algorithm 3	Algorithm 4
Reference	(Breiman et al., 1984)	(Geurts et al., 2006)		This paper
split coordinate	Exact optimization	Exact optimization	Importance sampling	Branch-and-bound
split value	Exact optimization	Random selection	Random $\tau < 1 /$ Exact $\tau = 1$	Random $\xi > 0 /$ Exact $\xi = 0$

Table 2: Comparison of state-of-the-art methods, where we essentially replace the splitting value and coordinate optimization $\min_{(j_0, j_1, j_2)} \mathcal{L}(j_0, j_1, j_2)$ with a surrogate problem and support approximate choices of splitting values to allow more expressive complexity trade-offs.

Leverage score sampling (LS) uses a sample rate τ to shrink the search space size from $d_1 d_2$ down to $\tau d_1 d_2$ for constrained optimization (see Algorithm 3). When $\tau = 1$, LS reduces to exhaustive search. The subset \mathcal{D} of dimension pairs (j_1, j_2) is chosen from $\{1, 2, \dots, d_1\} \times \{1, 2, \dots, d_2\}$ following a LS (without replacement) scheme (Murray et al., 2023; Malik and Becker, 2018). Pairs with higher variance are preferred since they offer diversity and may benefit low-rank approximations for R_1, R_2 . The probability of choosing a constant-value dimension is zero. LS keeps the same asymptotic computational complexity but sacrifices optimal solutions for faster computation during the greedy search for splits. This per-split strategy also shares the spirit of the traditional `mtry`-strategy used in random forests (Mentch and Zhou, 2020) which searches `mtry` (rather than all) features.

Branch-and-bound optimization (BB) considers a divide-and-conquer strategy for this optimization problem. In Algorithm 4, we introduce the tolerance ξ to divide the search space via the branch-and-bound strategy (Lawler and Wood, 1966; Morrison et al., 2016) and consider the optimization of (10) or (11) within the parameter tolerance ξ . When $\xi = 0$, this method reduces to regular exhaustive search. BB divides the entire space of $d_1 d_2$ potential splits into smaller search subspaces (i.e., branching). For each subspace, it estimates a bound on the quality of the best split coordinates (minimizing the chosen criterion) that can be found. If this estimated bound is worse than the best split (within the prespecified tolerance ξ) found so far, the subspace is excluded from further consideration (i.e., bounding). This method efficiently narrows the search to the most relevant splits and provides a practical alternative to exhaustive search at the price of possible local minima. To support our claim, Figure 2 shows that in the zero-noise cases, both LS and BB tend to have larger MSE compared to exhaustive search, regardless of the choice of leaf node fitting models, and the model quality deterioration becomes severe when the maximal depth increases. When there is more noise (i.e., lower signal-to-noise ratio in data), such differences in MSE between exhaustive search and BB/LS become less obvious. As rank of the leaf model increases, the performance of LS is less stable compared to BB. As the depth of the model increase, BB takes more time to fit compared to the linearly increasing sampling time of LS. Table 2 summarizes the difference between these fast search tree methods.

On one hand, our LS sampling (Algorithm 3) *randomly* chooses split coordinates but not the splits. It also serves as a surrogate importance measure for each coordinate combination. The LS design of choosing the optimal split among a fraction of all possible splits is related to that of extra-trees (Geurts et al., 2006). Extra-trees differ from classic decision trees in that instead of exhaustively optimizing for the optimal split, random splits are drawn using randomly selected features and the sub-optimal split among those candidates is chosen. When the candidate possible features is 1, this builds a totally random decision tree.

On the other hand, our BB (Algorithm 4) *deterministically* selects those split coordinates with the best approximation error at a certain tolerance level. BB exhibits a trade-off between the accuracy of the best pair (j_1, j_2) minimizing splitting criterion and search complexity but its quality will be affected by the additional tolerance hyper-parameter, which is not always straightforward to tune. BB also generalizes the classical constraint of limiting the maximal number of features used in all possible splits: limiting the number of features restricts the possible partitions induced by the tree, whereas BB also ensures that the “resolution” of tree-induced partition will not exceed a certain tolerance.

C Algorithms for Fitting Tensor Trees

Algorithm 2: Fitting vector-input decision tree regressor with SSE criterion (3).

Result: Train a vector-input single decision tree regressor and predict with it

```

1 Function  $\text{fit}(\mathbf{X} \in \mathbb{R}^{n \times d}, y \in \mathbb{R}^n)$ : begin
2   Initialize root node
3   for  $node$  in  $tree$  do
4     Calculate for all potential splits along each column  $j_1 \in \{1, 2, \dots, d\}$ : Find
       $\arg \min_{j_0 \in \{1, \dots, n\}, j_1 \in \{1, \dots, d\}} SSE(j_0, j_1)$ ;
5     With the minimizer  $(j_0^*, j_1^*)$  we split the dataset on the chosen column  $j_1^*$  and
      splitting value  $\mathbf{X}[j_0^*, j_1^*]$ , creating left and right child nodes using data in
       $R_1, R_2$ ;
6   end
7   Fit the chosen mean/CP/Tucker models at each of the leaf nodes.
8 end

```

Algorithm 3: Method 1: Leverage score sampling for fitting tensor input decision tree regressor with low-rank splitting criteria (10) and (11).

Result: Train a tensor input single decision tree regressor with leverage score sampling

```

1 Function  $\text{fit}(\mathbf{X} \in \mathbb{R}^{n \times d_1 \times d_2}, y \in \mathbb{R}^n)$ :
2 begin
3   Initialize root node and sample_rate  $\tau \in (0, 1]$  (when  $\tau = 1$  there is no
      subsampling). Compute the variance matrix  $\mathbf{V} = (\mathbf{X}[:, i, j])_{i, j=1}^{d_1, d_2}$ ;
4   for  $node$  in  $tree$  do
5     Take a random subset  $D \subset \{1, 2, \dots, d_1\} \times \{1, 2, \dots, d_2\}$  of cardinality  $\tau d_1 d_2$ 
      such that the probability of selecting dimension pair  $(j_1, j_2)$  is proportional
      to  $\mathbf{V}_{j_1, j_2}$ ;
6     Calculate for all potential splits along each dimension pair  $(j_1, j_2) \in D$ : Find
       $\arg \min_{j_0 \in \{1, \dots, n\}, (j_1, j_2) \in D} LAE(j_0, j_1, j_2)$  or  $LRE(j_0, j_1, j_2)$ ;
7     With the minimizer  $(j_0^*, j_1^*, j_2^*)$  we split the dataset on the chosen dimension
      pair  $(j_1^*, j_2^*)$  and splitting value  $\mathbf{X}[j_0^*, j_1^*, j_2^*]$ , creating left and right child
      nodes using data in  $R_1, R_2$ ;
8   end
9   Fit the chosen mean/CP/Tucker models at each of the leaf nodes.
10 end

```

Algorithm 4: Method 2: Branch-and-bound optimization for fitting tensor input decision tree regressor with low-rank splitting criteria (10) and (11).

Result: Train a tensor input single decision tree regressor with branch-and-bound optimization

```

1 Function fit( $\mathbf{X} \in \mathbb{R}^{n \times d_1 \times d_2}$ ,  $\mathbf{y} \in \mathbb{R}^n$ ):
2 begin
3   Initialize root node;
4   for node in tree do
5     Take the full set  $D = \{1, 2, \dots, d_1\} \times \{1, 2, \dots, d_2\}$  of cardinality  $d_1 d_2$ ;
6     Calculate for all potential splits along each dimension pair  $(j_1, j_2) \in D$ : Use
     best_idx as  $(j_1, j_2)$  from the return of BnB_minimize(LAE, D,  $\xi$ ) or
     BnB_minimize(LRE, D,  $\xi$ );
7     With the minimizer  $(j_0^*, j_1^*, j_2^*)$  we split the dataset on the chosen dimension
     pair  $(j_1^*, j_2^*)$  and splitting value  $\mathbf{X}[j_0^*, j_1^*, j_2^*]$ , creating left and right child
     nodes using data in  $R_1, R_2$ ;
8   end
9   Fit the chosen mean/CP/Tucker models at each of the leaf nodes.
10 end
11 Function BnB_minimize( $obj, D, \xi$ ):
12 begin
13   Set best_obj to infinity; Set initial bounds  $D$  for tensor dimensions and append
      $D$  to queue;
14   while queue is not empty do
15      $D_c = \text{queue.pop}(0)$ ;
16     mid_feature_index = tuple((b[0] + b[1]) // 2 for b in current  $D_c$ );
17     Calculate  $obj$  at mid_feature_index;
18     if  $obj < \text{best\_obj}$  then Update  $\text{best\_obj}$ ,  $\text{best\_idx}$ ;
19     for i in range(len( $D_c$ )) do
20       if  $D_c[i][1] - D_c[i][0] > \text{tolerance } \xi$  then
21         mid_point =  $(D_c[i][0] + D_c[i][1]) // 2$ ;
22         left_bounds = right_bounds =  $D_c$ ;
23         left_bounds[i] =  $(D_c[i][0], mid\_point)$ ;
24         right_bounds[i] =  $(mid\_point + 1, current\_bounds[i][1])$ ;
25         queue.append(left_bounds, right_bounds);
26         break;
27       end
28     end
29   end
30   Return  $\text{best\_obj}$ ,  $\text{best\_idx}$  ;
31 end

```

D Pruning Experiment

Here we show the effect of pruning using the tensor-input scalar-output synthetic function

$$f(\mathbf{X}) = \begin{cases} 5 & \text{if } \mathbf{X}[:, 0, 1, 0]^{36} \geq 0.4 \\ -1 & \text{if } \mathbf{X}[:, 0, 1, 0] < 0.4 \text{ and } \mathbf{X}[:, 2, 2, 0] \geq 0.65, \end{cases} \quad (21)$$

which can be represented by a tree with three leaves. As shown in Figure 7, we fit trees using the variance splitting criterion and various pruning parameter values α . First we observe that for all shown α values that the MSE decreases with tree’s maximal depth, and that this decrease levels off once the maximal depth is two or larger. We also see that trees without pruning ($\alpha = 0$) can grow to have many leaves, but once pruning is introduced ($\alpha > 0$), trees with $\text{max_depth} \geq 2$ are typically pruned to have three or four leaves, especially at $\alpha = 0.1$ (i.e., the largest tested α value). Hence, in this example, an appropriately large α value induces sufficient pruning for trees to have the “correct” number of leaves.

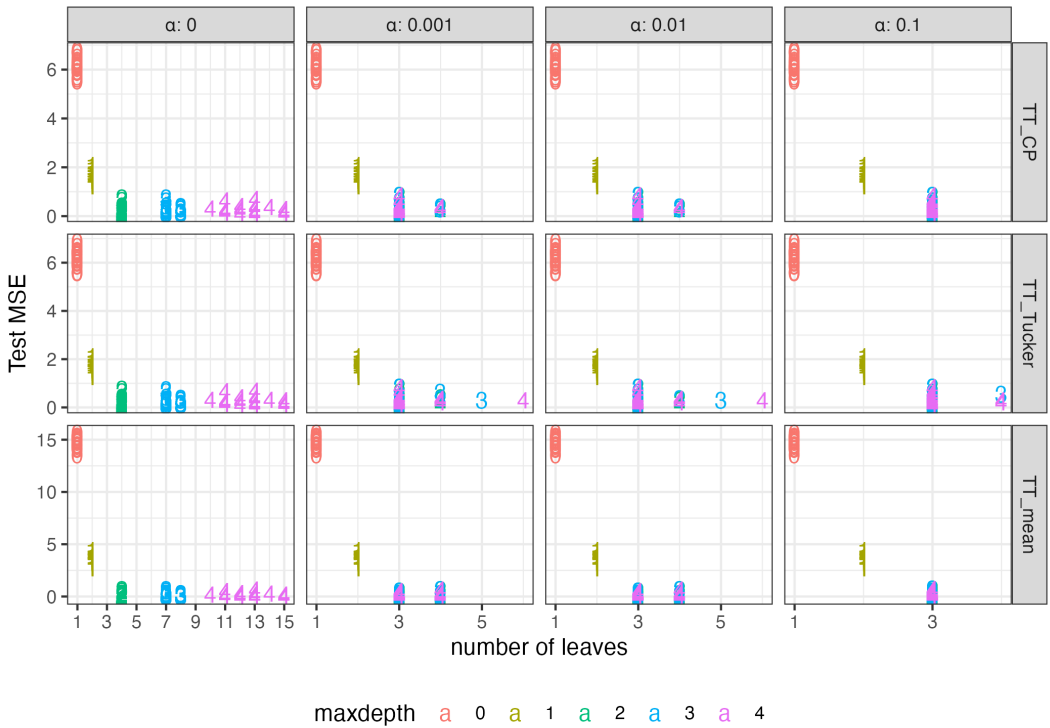


Figure 7: Out-of-sample MSE of trees trained on data generated by first sampling (500, 4, 4, 4) input tensor \mathbf{X} uniformly randomly from $[0, 1]$ and then evaluating the function (21) at the input tensor before adding i.i.d. Gaussian noise with mean zero and variance 0.1. The figure shows 20 replicates for each combination of α , max_depth , and leaf model.

E Boosted Trees

Boosting is an ensemble learning technique that enhances model performance by combining multiple weak learners, usually decision trees, into a strong learner. This method sequentially trains base models, with each new model correcting the errors of the previous ones, thus reducing bias and variance. Pioneering boosting algorithms include AdaBoost (Freund and

Schapire, 1997), which adjusts weights of misclassified instances, and Gradient Boosting (Friedman, 2001; Friedman et al., 2004), which fits new models to residual errors.

Before describing boosted trees in detail, we first introduce a different tree ensemble method called Random Forests (RFs). Random Forests (Breiman, 2001; Amit and Geman, 1997) create an ensemble of independent decision trees using bootstrap samples and random feature subsets, enhancing diversity and robustness through randomization over the feature space. For a given set of n data pairs (\mathbf{X}_i, y_i) , where \mathbf{X}_i are input tensors and y_i are scalar responses, a RF builds B trees. Each tree is trained on a bootstrap sample of the data, and at each split, a random subset of features is considered as shown in Algorithm 5. This approach reduces the variance of the model by averaging the predictions of independently trained trees, which helps mitigate overfitting. The main challenge of ensembling trees is ensuring that the trees are diverse enough to capture different patterns in the data without making inconsistent predictions.

Although RFs combined with TT (See Algorithm 5) are powerful, its performance on predicting entries in a tensor output is not ideal. We focus on boosting methods, which iteratively improve the model by focusing on previously mispredicted instances. Boosting constructs trees sequentially, where each new tree corrects errors from the previous ones, leading to a strong aggregated model. Therefore, the concept behind boosting diverges fundamentally from RF. Boosting does not aggregate weak learners; instead, it averages the predictions of strong learners. This method is particularly effective for our tensor regression tree models, as detailed in the following sections. Gradient Boosting (Friedman, 2001) constructs an ensemble of decision trees sequentially, where each new tree is trained to correct the errors of the existing ensemble. Unlike RFs, where trees are built independently, GB involves a functional gradient descent approach to minimize a specified loss function (Hastie et al., 2009).

In the general case, gradient boosting involves computing “pseudo-residuals,” which are the negative gradients of the loss function with respect to the model’s predictions. For a given loss function $L(y, F(\mathbf{X}))$, the pseudo-residuals at iteration b are given by:

$$r_i^{(b)} = - \left[\frac{\partial L(y_i, F(\mathbf{X}_i))}{\partial F(\mathbf{X}_i)} \right]_{F(\mathbf{X})=F_{\text{GB}}^{(b-1)}(\mathbf{X})}.$$

Each new tree g_b is then fit to these pseudo-residuals, and the model is updated as follows:

$$F_{\text{GB}}^{(b)}(\mathbf{X}) = F_{\text{GB}}^{(b-1)}(\mathbf{X}) + \eta g_b(\mathbf{X}; T_b, M_b),$$

where η is a learning rate that controls the contribution of each tree. The new tree minimizes

the loss function:

$$\operatorname{argmin}_{T_b, M_b} \sum_{i=1}^n L \left(y_i, F_{\text{GB}}^{(b-1)}(\mathbf{X}_i) + g_b(\mathbf{X}_i; T_b, M_b) \right).$$

In our case, we focus on a simpler version of tree boosting algorithm, which uses the squared error loss (for the scalar response y). This approach iteratively fits trees to the residuals of the previous trees without explicitly computing pseudo-residuals. For a set of n data pairs (\mathbf{X}_i, y_i) , one popular tree boosting model constructs an additive series of m regression trees:

$$F_{\text{GB}}(\mathbf{X}) = \sum_{b=1}^m g_b(\mathbf{X}; T_b, M_b), \quad (22)$$

where each tree $g_b(\mathbf{X}; T_b, M_b)$ is fit to the residuals of the previous ensemble:

$$r_i^{(b)} = y_i - F_{\text{GB}}^{(b-1)}(\mathbf{X}_i). \quad (23)$$

Each new tree is trained to minimize the squared error loss on these residuals:

$$\operatorname{argmin}_{T_b, M_b} \sum_{i=1}^n \left(r_i^{(b)} - g_b(\mathbf{X}_i; T_b, M_b) \right)^2.$$

By sequentially fitting trees to the residuals, the forward-stagewise fitting approach builds a strong aggregated model, effectively capturing the complex patterns in the data while mitigating overfitting. This method is particularly suitable for our tensor regression tree models.

In addition, Bayesian regression trees (Chipman et al., 1998; Denison et al., 1998; Chipman et al., 2010, 2012) extend this approach by placing a prior distribution on the space of possible trees and their hyper-parameters like splitting coordinates and values, hence providing uncertainty quantification over predictions. Posterior distributions of the trees are then explored and updated using Markov chain Monte Carlo (MCMC) methods. The Bayesian approach allows for full posterior inference, including point and interval estimates of the unknown regression function and the effects of potential predictors (Pratola et al., 2014; Pratola, 2016; Luo and Pratola, 2022). Bayesian Additive Regression Trees (BART), introduced by Chipman et al. (2010), combine Bayesian methods with boosting principles, modeling responses as a sum of regression trees and providing a probabilistic framework with uncertainty quantification.

F Proof of Proposition 1

Proof. Since each decomposition when constructing the tree structure takes no more than $N^* < \infty$ iterations, it suffices to consider per iteration complexity as stated in Lemmas 1 and 2.

(1) The computational complexity at any node t with n_t samples is $\mathcal{O}(n_t d_1 d_2)$ for finding the best split. In a balanced binary tree with n samples in $\mathbb{R}^{d_1 \times d_2}$, i -th level has 2^i nodes, each processing $\mathcal{O}(n 2^{-i})$ samples. The complexity per node is then $\mathcal{O}(n 2^{-i} \cdot d_1 d_2)$. Hence, the total complexity for level i is $2^i \cdot \mathcal{O}(n 2^{-i} \cdot d_1 d_2) = \mathcal{O}(n d_1 d_2)$. Summing over all K levels, the overall complexity is $\mathcal{O}(n \cdot d_1 d_2 \cdot \log k)$.

(2) Now the total complexity for level i is $2^i \cdot \mathcal{O}(d_1 d_2 n 2^{-i}) \cdot \mathcal{O}(d_1 d_2 n 2^{-i})$. The first factor ($d_1 d_2 n 2^{-i}$) comes from the search of all samples at each coordinate combination in each node at this level. The second factor ($d_1 d_2 n 2^{-i}$) comes from setting $R = n 2^{-i}$ and $K = 2$ in Lemma 1 since the maximum rank of tensor decomposition cannot exceed the number of sample sizes. Summing over all $\log k$ levels, the overall complexity is $\mathcal{O}(n^2 d_1^2 d_2^2 \cdot \log k)$.

(3) Now the total complexity for level i is

$$2^i \cdot \mathcal{O}(d_1 d_2 n 2^{-i}) \cdot \mathcal{O}(n 2^{-i} d_1 d_2 \cdot \min(d_1 d_2, n 2^{-i}) + n 2^{-i} d_1 d_2 \cdot \min(n 2^{-i} d_1, n 2^{-i} d_2, d_2, d_1)) .$$

The first factor ($d_1 d_2 n 2^{-i}$) comes from the search of all samples at each coordinate combination in each node at this level. The second factor come from setting $R = n 2^{-i}$ and $K = 2$ in Lemma 2. Summing over all $\log k$ levels, the overall complexity is

$$\mathcal{O}(\log k \cdot n^2 d_1^2 d_2^2 \cdot (\min(d_1 d_2, n) + \min(nd_1, nd_2, d_2, d_1))) .$$

Then we can simplify the term $\min(nd_1, nd_2, d_2, d_1)$ to $\min(d_2, d_1)$ since we know that $n \geq 1$ by assumption. \square

G Proof of Lemma 2

Proof. The argument is as follows, since the complexity bottleneck per iteration comes from the SVD step:

$$\begin{aligned}
& \mathcal{O} \left(\min \left\{ n \prod_{j=1}^K d_j'^2, n^2 \prod_{j=1}^K d_j' \right\} + \sum_{i=1}^K \min \left\{ R^2 \cdot d_i \prod_{j \neq i} d_j'^2, R \cdot d_i^2 \prod_{j \neq i} d_j' \right\} \right) \\
& \asymp \mathcal{O} \left(\min \left\{ n \prod_{j=1}^K d_j'^2, n^2 \prod_{j=1}^K d_j' \right\} + \sum_{i=1}^K \min \left\{ R^2 \cdot \frac{d_i}{d_i'^2} \prod_{j=1}^K d_j'^2, R \cdot \frac{d_i^2}{d_i'} \prod_{j=1}^K d_j' \right\} \right) \\
& \asymp \mathcal{O} \left(\min \left\{ n \prod_{j=1}^K d_j^2, n^2 \prod_{j=1}^K d_j \right\} + \sum_{i=1}^K \min \left\{ R^2 \cdot \frac{1}{d_i} \prod_{j=1}^K d_j^2, R \cdot d_i \prod_{j=1}^K d_j \right\} \right) \text{ since } d_i' \asymp d_i, \\
& \lesssim \mathcal{O} \left(n \prod_{j=1}^K d_j^2 + \sum_{i=1}^K R \cdot d_i \prod_{j=1}^K d_j \right)
\end{aligned}$$

Because $R < n$, in the preceding line the first summand dominates the second summand. We conclude the proof by noting that $\prod_{i=1}^K d_i^2 \leq (\max_i d_i)^{2K}$. \square

H Proof of Theorem 3

Proof. The proof is almost identical to the proof of Theorem 4.2 in Klusowski and Tian (2024) since when minimizing (9) and splitting at each interior node we indeed “flatten” the input tensor \mathbf{X} along its second and third coordinates. We consider the maximum impurity gain $IG(t)$ for N_t samples in node t to decrease the empirical risk for the regressor g

$$\hat{\mathcal{R}}_t(g) = \frac{1}{N_t} \sum_{\mathbf{X}^{(n)}[i,:,:] \in t} \mathcal{L}(y_i, g(\mathbf{X}^{(n)}[i,:,:])),$$

for the chosen loss function \mathcal{L} (e.g., (9)) in the parent node t . When we split node t into left and right nodes

$$\begin{aligned}
t_L &:= \{\mathbf{X} \in t: \mathbf{X}[:, j_1, j_2] \leq s\}, N_{t_L} = \#\{\mathbf{X}^{(n)}[i,:,:] \in t_L\}, \\
t_R &:= \{\mathbf{X} \in t: \mathbf{X}[:, j_1, j_2] > s\}, N_{t_R} = \#\{\mathbf{X}^{(n)}[i,:,:] \in t_R\}
\end{aligned}$$

we have an analog to Lemma A.1 in Klusowski and Tian (2024) for the ℓ_2 inner product between multivariate functions u and v . At node t , this inner product is evaluated only at

those observed locations $\mathbf{X}^{(n)}[i, :, :] \in t$:

$$\begin{aligned} \langle u, v \rangle_t &:= \frac{1}{N_t} \cdot \sum_{\mathbf{X}^{(n)}[i, :, :] \in t} u(\mathbf{X}^{(n)}[i, :, :]) \cdot v(\mathbf{X}^{(n)}[i, :, :]) \\ &= \frac{1}{N_t} \cdot \sum_{\mathbf{X}^{(n)}[i, :, :] \in t} \sum_{j, k} u(\mathbf{X}[i, j, k]) \cdot v(\mathbf{X}[i, j, k]) \text{ for (9).} \end{aligned}$$

The key idea in proving the impurity gain lower bound is to use a linear interpolator over the domain \mathbb{R} indexed by $\mathbb{N} \times \mathbb{N}$, for the ordered statistics $\mathbf{X}[(1), j_1, j_2] \leq \dots \leq \mathbf{X}[(n), j_1, j_2]$, to control the empirical risk. To attain this goal, we define the probability measure $\Pi(j_1, j_2, s)$ for splitting point s and variables $\mathbf{X}[:, j_1, j_2]$ where its RN derivative with respect to the counting measure on $\mathbb{N} \times \mathbb{N}$ and the Lebesgue measure on \mathbb{R} (this is still defined on \mathbb{R} not $\mathbb{R}^{d_1 \times d_2}$ since the split still happens by one threshold s) can be written as

$$\frac{d\Pi(j_1, j_2, s)}{d(j_1, j_2) \times ds} := \frac{|Dg_{j_1, j_2}(s)| \sqrt{N_{t_L} N_{t_R} / N_t^2}}{\sum_{i_1=1}^{d_1} \sum_{i_2=1}^{d_2} \int_{\mathbb{R}} |Dg_{i_1, i_2}(s')| ds'}$$

$$Dg_{j_1, j_2}(s) = \begin{cases} \frac{g_{j_1, j_2}(\mathbf{X}[(i+1), j_1, j_2]) - g_{j_1, j_2}(\mathbf{X}[(i), j_1, j_2])}{\mathbf{X}[(i+1), j_1, j_2] - \mathbf{X}[(i), j_1, j_2]} & \mathbf{X}[(i), j_1, j_2] < s < \mathbf{X}[(i+1), j_1, j_2] \\ 0 & \text{otherwise} \end{cases}.$$

Using these bi-indexed linear interpolators $Dg_{j_1, j_2}(s)$ as piece-wise density functions, we obtain an impurity gain formula for a tensor-input tree when splitting with the SSE criterion and fitting with mean leaf models.

Analog of Lemma 4.1 (Tensor Input Case): Let $g \in \mathcal{G}_1$ and $K \geq 1$ be any depth. For any terminal node t of the tree T_{K-1} such that $\hat{\mathcal{R}}_t(g_{T_{K-1}}) > \hat{\mathcal{R}}_t(g)$, we have

$$IG(t) \geq \frac{(\hat{\mathcal{R}}_t(\hat{g}_{T_{K-1}}) - \hat{\mathcal{R}}_t(g))^2}{V^2(g)}$$

where $V(g) = \|g\|_{TV}$ is a complexity constant dependent on g .

Next, we proceed with the proof of Theorem 3, which is an analog of Theorem 4.2 of Klusowski and Tian (2024). Since the output is still scalar, we use recursion for empirical risk reduction and get the total risk

$$\hat{\mathcal{R}}(g_{T_K}) = \hat{\mathcal{R}}(g_{T_{K-1}}) - \sum_{t \in T_{K-1}} \frac{N_t}{N} IG(t)$$

where $t \in T_{K-1}$ means that t is a terminal node of tree T_{K-1} . By the above tensor analog of Lemma 4.1, the total impurity gain over all terminal nodes $t \in T_{K-1}$ such that $\hat{\mathcal{R}}_t(g_{T_{K-1}}) > \hat{\mathcal{R}}_t(g)$ is bounded by

$$\sum_{t \in T_{K-1} : \hat{\mathcal{R}}_t(g_{T_{K-1}}) > \hat{\mathcal{R}}_t(g)} \frac{N_t}{N} IG(t) \geq \sum_{t \in T_{K-1} : \hat{\mathcal{R}}_t(g_{T_{K-1}}) > \hat{\mathcal{R}}_t(g)} \frac{N_t}{N} \frac{(\hat{\mathcal{R}}_t(\hat{g}_{T_{K-1}}) - \hat{\mathcal{R}}_t(g))^2}{V^2(g)}.$$

Applying Jensen's inequality to the sum, we get

$$\begin{aligned} \sum_{t \in T_{K-1} : \hat{\mathcal{R}}_t(g_{T_{K-1}}) > \hat{\mathcal{R}}_t(g)} \frac{N_t}{N} (\hat{\mathcal{R}}_t(\hat{g}_{T_{K-1}}) - \hat{\mathcal{R}}_t(g))^2 &\geq \left(\sum_{t \in T_{K-1} : \hat{\mathcal{R}}_t(g_{T_{K-1}}) > \hat{\mathcal{R}}_t(g)} \frac{N_t}{N} (\hat{\mathcal{R}}_t(\hat{g}_{T_{K-1}}) - \hat{\mathcal{R}}_t(g)) \right)^2 \\ &\geq \left(\sum_{t \in T_{K-1}} \frac{N_t}{N} (\hat{\mathcal{R}}_t(\hat{g}_{T_{K-1}}) - \hat{\mathcal{R}}_t(g)) \right)^2. \end{aligned}$$

The global excess risk can be defined as

$$E_K := \hat{\mathcal{R}}(g_{T_K}) - \hat{\mathcal{R}}(g).$$

We can rewrite the total impurity gain as

$$\sum_{t \in T_{K-1}} \frac{N_t}{N} (\hat{\mathcal{R}}_t(\hat{g}_{T_{K-1}}) - \hat{\mathcal{R}}_t(g)) = E_{K-1}.$$

Combining the results from steps above, we have

$$E_K \leq E_{K-1} \left(1 - \frac{E_{K-1}}{V^2(g)} \right).$$

By induction, we iterate this inequality to obtain

$$E_K \leq \frac{V^2(g)}{K+3}.$$

Finally, substituting back into the empirical risk, we obtain

$$\hat{\mathcal{R}}(g_{T_K}) \leq \hat{\mathcal{R}}(g) + \frac{V^2(g)}{K+3}.$$

Taking the infimum over all functions g , we get

$$\hat{\mathcal{R}}(g_{T_K}) \leq \inf_{g \in \mathcal{G}_1} \left\{ \hat{\mathcal{R}}(g) + \frac{V^2(g)}{K+3} \right\}.$$

Hence, we have proved an analog of Theorem 4.2 for the tensor input case, where the only difference is the statement and definitions used in the analog of Lemma 4.1. \square

I Algorithms for Ensembles of Trees

Leaf model m_j	Split criteria	variance	clustering	low-rank
Sample average of the y		max_depth	max_depth, cluster_method	split_rank, max_depth
CP regression on y		max_depth, CP_reg_rank	max_depth, cluster_method, CP_reg_rank	split_rank, max_depth, CP_reg_rank
Tucker regression on y		max_depth, Tucker_reg_rank	max_depth, cluster_method, Tucker_reg_rank	split_rank, max_depth, Tucker_reg_rank

Table 3: Supported combination methods: TensorDecisionTreeRegressor and associated parameters, and how it generalizes existing models.

Algorithm 5: Random Forest with Tensor Input

Result: Forest of decision trees $\{T_t\}$

- 1 **Input:** Tensor data $\mathbf{X} \in \mathbb{R}^{n \times p_1 \times p_2 \times \dots \times p_d}$, Target values $y \in \mathbb{R}^n$, Number of trees T ;
- 2 **for** $t \leftarrow 1$ **to** T **do**
- 3 $(X_t, y_t) \leftarrow$ Bootstrap sample from (X, y) ;
- 4 $T_t \leftarrow$ Train a decision tree on (X_t, y_t) with random subsampling of predictors at root node;
- 5 Store all observations in each leaf of T_t ;
- 6 Fit the chosen mean/CP/Tucker models at each of the leaf nodes of T_t ;
- 7 **end**
- 8 $\mathbf{y}_i^{pred} = \sum_{t=1}^T F_t(\mathbf{X}^{(n)}[i, :, :])$;

Algorithm 6: Generalized Boosting Regressor with Optional AdaBoost-Like Resampling

Result: Train a generalized boosting regressor model and predict with it

1 Function GeneralizedBoostingRegressor($\mathbf{X} \in \mathbb{R}^{n \times d_1 \times d_2}$, $\mathbf{y} \in \mathbb{R}^n$, M , η , $presample$):

2 begin

3 Initialize $F_0(x)$ to the mean of \mathbf{y} ;

4 **for** $m = 1$ **to** M **do**

5 Compute residuals: $r_{im} = y_i - F_{m-1}(\mathbf{X}^{(n)}[i, :, :])$ for all i ;

6 **if** $presample > 0$ **then**

7 Sample indices according to weights:
 $\mathbf{I}_{resample} \sim \text{Sample}(\text{Indices}, \text{Weights}, \text{Size} = n \times presample)$;

8 $\mathbf{h}_m = \text{fit}(\mathbf{X}[\mathbf{I}_{resample}, :, :], r_{im}[\mathbf{I}_{resample}])$;

9 Update weights: Weights = Weights $\times \exp(|r_{im}|)$;

10 Normalize weights: Weights = Weights / \sum Weights;

11 **else**

12 **end**

13 **for** each sample i **do**

14 $\mathbf{y}_i^{pred} = F_{m-1}(\mathbf{X}^{(n)}[i, :, :]) + \eta \mathbf{h}_m(\mathbf{X}^{(n)}[i, :, :])$;

15 **end**

 Update $F_m(x) = F_{m-1}(x) + \eta \mathbf{h}_m(x)$;

16 **end**

17 **return** $F_M(x)$;

18 **end**

19 **end**

J Training time for fixed N , increasing d_2

Here we perform an experiment to illustrate how the training time of our and other tensor methods increases as tensor dimension d_2 increases under a fixed value of the sample size $N = 100$ and tensor dimension $d_1 = 25$. The data is generated in the same way as in the experiments in Figure 5 of the main text.

Figure 8 shows that as tensor dimension d_2 increases, the GP-based methods (TensorGP and GPST) have the largest increase and total training time, followed by the TT methods, then by CP, then by Tucker. (All TT models with the same max_depth have roughly the same training time, so for each depth we show only TT_CP without pruning. Also, we show only max_depth=3,6 to reduce visual clutter.) These results complement and are similar in spirit to the findings from our analysis of Figures 5 and 6 in the main text.

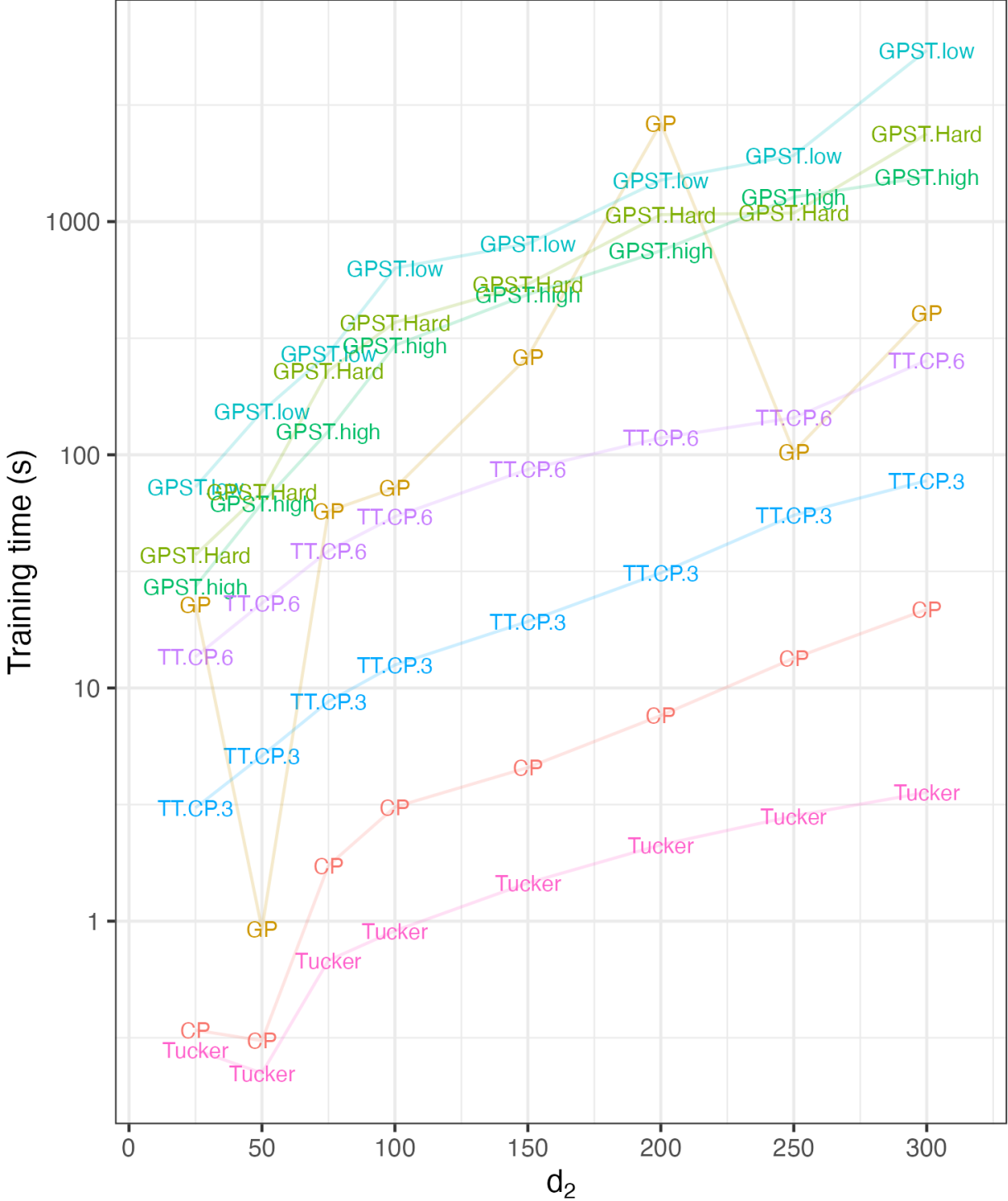


Figure 8: In-sample and out-of-sample training time (seconds) against the second tensor dimension d_2 for the experiments in Figure 5. Here the sample size is $N = 100$ and the first tensor dimension is $d_1 = 25$. For TT models, we experiment with `max_depth=3,6` and select $\alpha = 0.5$ in (17) and perform only one fit on an AMD Ryzen 5 3600XT 6-core, 12-thread processor.

K Out-of-sample MSE with entrywise input noise

Here we perform an experiment to illustrate the robustness of our and other tensor methods to independent entrywise noise in the input tensors. The experiment includes various levels of input noise; we set the standard deviation of each entry’s noise equal to the value `input_noise_sd` times the input tensor’s standard deviation.

Figure 9 shows that TT_CP and TT_Tucker with pruning are robust to `input_noise_sd` up to 0.3, regardless of the `max_depth`. We also see that without pruning, TT_CP and TT_Tucker perform dramatically worse as depth increases, which indicates that the pruning procedure is correctly decreasing the depth of the tree to mitigate overfitting the input noise. Once `input_noise_sd` equals 1, all methods (except for TT_mean with pruning, which has a large test MSE even with no input noise) display a noticeable increase in test MSE, indicating that TT_CP and TT_Tucker with pruning are among the most robust methods tested in this experiment.

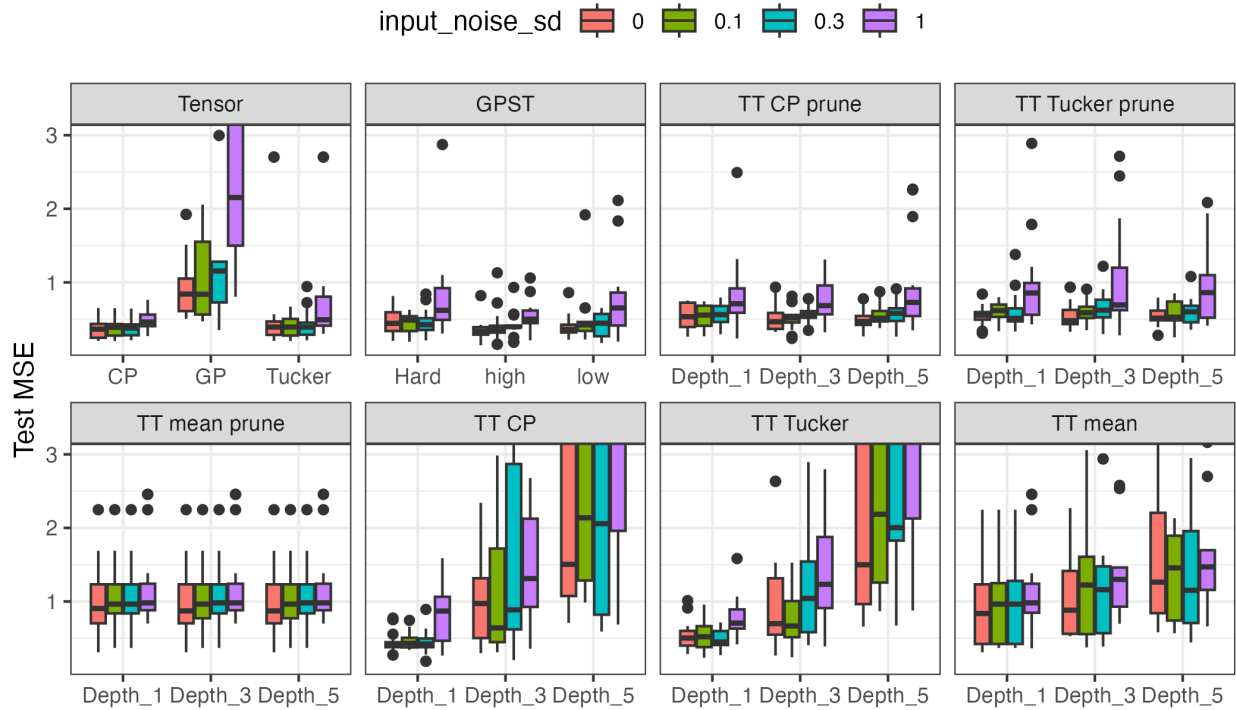


Figure 9: Test MSE for the experiments in Figure 5 for input tensors of size $(N, d_1, d_2) = (100, 25, 25)$. Zero-mean Gaussian noise is added entrywise to the input tensors so that each model is provided only noisy versions of the input tensors. The noise standard deviation is `input_noise_sd` multiplied by the input’s standard deviation. For TT models, we experiment with `max_depth=1,3,5` and select $\alpha = 0.5$ in (17) and perform 20 replicates.

L MSE comparison to existing forest methods

This section explores the performance of regression models — Fréchet Random Forest (FRF, bootstrap ratio = 0.75 and other parameters are default values), global Fréchet regression (GRF), and Tensor Tree (TT) with gradient boosting (GB) — on synthetic datasets. For code implementation, `pyfrechet` (<https://github.com/matthieubulte/pyfrechet>) by Bulté and Sørensen (2024) only supports 2-mode tensor as a Fréchet space input and scalar outputs, since their focus is spherical data. `FrechForest` (CRAN package, last maintained 2019, used by Capitaine et al. (2024); Qiu et al. (2024)) supports mainly curves as Fréchet space input and scalar output, but also supports 2- and 3-mode tensors. In contrast, our open-source implementation supports up to 4-mode tensor inputs and outputs, with improved efficiency, significantly extending the usability of the existing tensor nonparametric regression software.

The first experiment explores different noise levels and number of trees in the ensemble methods. The target variable is $y = 2 \cdot X[:, 0] \cdot X[:, 2] + 3 \cdot X[:, 1] \cdot X[:, 2] \cdot X[:, 3] + \varepsilon$, where ε is Gaussian noise with a configurable noise variance. The input X is an $n = 1000, d = 5$ matrix with i.i.d. standard uniform entries, and we embed X as a 3-tensor (adding an all-zero third dimension to be compatible with TT implementation) tailored to simulate structured data scenarios. For the parameter settings of the tested methods, `pyfrechet`'s FRF has no option for limiting each tree's maximum depth, so we set the minimum number of observations in each leaf node to two. For `FrechForest`'s FRF we use the default parameter settings other than the number of trees to grow. The TT models use `max_depth=4`, `split_rank=4` and full exploration rate $\alpha = 1$, and we also execute TTentrywise GB ensembles (with maximum depth 4 and at least two observations per leaf node) in order to compete with the two mentioned ensemble methods. (If desired, Algorithm 5 shows how to train a random forest using TT.) The models are trained and evaluated over 10 random seeds to ensure robustness in MSE (on a held-out test data) and time measurements shown in Table 4. Comparing single-tree models, TT has competitive performance and fast fits compared to either FRF implementation with one tree. We expect that TT will outperform FRF for higher mode tensor inputs for a similarly simple input-response relationship, since higher mode tensors require more samples to have accurate estimates of Fréchet distances. Comparing ensemble methods, TT GB with 5 or 50 trees has larger test MSEs than FRF with the same number of trees. However, FRF seems to improve very little past 50 trees, whereas TT GB with 500 trees has a much smaller test MSE than FRF with any of the tested number of trees. Thus, of all tested ensemble methods, TT GB is able to provide by far the smallest test MSE for this scenario.

method	# trees	noise variance 0	noise variance 0.01	noise variance 0.1
TT	1	0.108 (1s)	0.089 (1s)	0.138 (1s)
TTtrywise GB	5	1.136 (12s)	1.135 (11s)	1.138 (9s)
TTtrywise GB	50	0.510 (33s)	0.521 (41s)	0.516 (42s)
TTtrywise GB	250	0.039 (196s)	0.038 (221s)	0.038 (204s)
TTtrywise GB	500	0.015 (588s)	0.014 (574s)	0.019 (557s)
GFR	n/a	0.258 (1s)	0.194 (1s)	0.199 (2s)
pyfrechet FRF	1	0.098 (4s)	0.077 (4s)	0.114 (5s)
pyfrechet FRF	50	0.055 (24s)	0.045 (19s)	0.067 (15s)
pyfrechet FRF	250	0.052 (111s)	0.043 (109s)	0.066 (114s)
pyfrechet FRF	500	0.047 (246s)	0.049 (245s)	0.068 (241s)
FrechForest FRF	1	0.145 (2s)	0.150 (2s)	0.176 (2s)
FrechForest FRF	5	0.054 (4s)	0.055 (4s)	0.071 (4s)
FrechForest FRF	50	0.033 (23s)	0.033 (23s)	0.044 (23s)
FrechForest FRF	250	0.031 (108s)	0.031 (108s)	0.042 (108s)
FrechForest FRF	500	0.031 (210s)	0.030 (209s)	0.042 (210s)

Table 4: Out-of-sample MSEs and fit-predict time (seconds) for each forest method with different number of trees in the ensemble method.

The second experiment compares TT with one tree against (FrechForest's) FRF for higher mode tensor inputs and a more complex input-response relationship. To be compatible with FrechForest, we reduce the three channels to one in the simulation code in the experiments in Figure 5 of the main text in order to reduce the number of modes of the input tensors from 4 to 3. This 3-tensor input has dimensions $n = 750$ and $d_1 = d_2 = 25$. The test MSE is computed on a held-out set with $n = 250$. Figure 10 shows that with pruning, TT_CP and TT_Tucker with max_depth 1 have a similar test MSE to FRF with at least five trees but fit much faster (FRF with 250 trees took around 11 minutes to fit). These two TT methods also have about half of the test MSE and half of the training time than FRF with one tree. In this scenario, TT with one tree is faster to fit and has competitive performance to FRF with any number of trees.

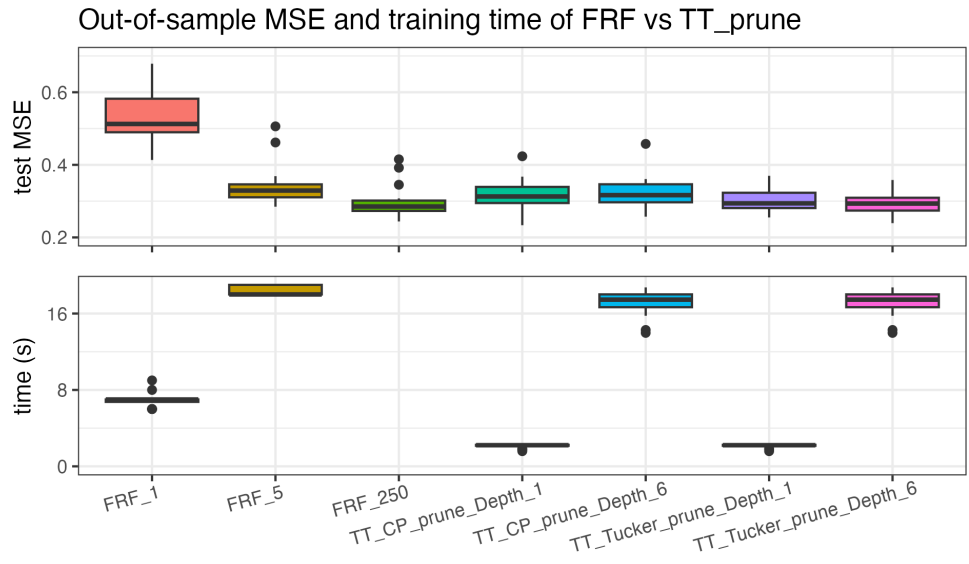


Figure 10: Test MSE for modified experiments in Figure 5 for input tensors of size $(N, d_1, d_2) = (1000, 25, 25)$. The number after the “Depth_” label indicates the max_depth of the TT method. The number after the “FRF_” label indicates the number of trees. All models are run with 20 replicates. Each FRF with 250 trees took about 11 minutes (660 seconds) to fit.

M RPE results comparing the rrr method to TT

Rank	rrr	rrrBayes	TTentrywise_CP	TTentrywise_Tucker	TTlowrank_CP	TTlowrank_Tucker
2	143 ± 9	136 ± 9	218 ± 3	223 ± 4	172 ± 2	3581 ± 79
3	172 ± 9	162 ± 7	219 ± 3	219 ± 3	132 ± 2	3633 ± 84
4	177 ± 10	171 ± 9	219 ± 3	219 ± 3	134 ± 2	3678 ± 90
5	178 ± 5	170 ± 5	216 ± 3	216 ± 3	133 ± 2	3628 ± 92
6	174 ± 7	207 ± 24	219 ± 4	219 ± 4	137 ± 2	3715 ± 106
7	260 ± 17	319 ± 24	219 ± 3	219 ± 3	138 ± 2	3659 ± 85

$$(a) \text{ Linear. } (d_1, d_2) = (3, 4). \ p_1 = 15. \ \mathbf{y}[:, i] = \begin{cases} \mathbf{X}[:, 0, 1] + \mathbf{X}[:, 1, 1] & \text{if } i \bmod 3 = 0 \\ \mathbf{X}[:, 1, 1] + \mathbf{X}[:, 2, 0] & \text{if } i \bmod 3 = 1. \\ \mathbf{X}[:, 2, 2] + \mathbf{X}[:, 0, 3] & \text{if } i \bmod 3 = 2 \end{cases}$$

Rank	rrr	rrrBayes	TTentrywise_CP	TTentrywise_Tucker	TTlowrank_CP	TTlowrank_Tucker
2	219 ± 5	209 ± 3	205 ± 2	206 ± 3	297 ± 2	1249 ± 18
3	231 ± 8	211 ± 4	205 ± 2	206 ± 3	260 ± 2	1265 ± 25
4	240 ± 9	218 ± 6	205 ± 2	206 ± 3	231 ± 3	1290 ± 27
5	241 ± 11	222 ± 8	205 ± 2	206 ± 3	200 ± 2	1279 ± 12
6	257 ± 8	240 ± 8	203 ± 2	204 ± 2	169 ± 2	1328 ± 23
7	288 ± 31	276 ± 32	205 ± 2	206 ± 3	261 ± 34	1332 ± 38

$$(b) \text{ Non-linear. } (d_1, d_2) = (3, 4). \ p_1 = 6. \ \mathbf{y}[:, i] = \sin(\mathbf{X}[:, i \bmod 3, i \bmod 4]).$$

Rank	rrr	rrrBayes	TTentrywise_CP	TTentrywise_Tucker	TTlowrank_CP	TTlowrank_Tucker
2	342 ± 69	326 ± 65	455 ± 36	464 ± 35	392 ± 43	204 ± 37
3	433 ± 91	404 ± 86	456 ± 36	465 ± 34	395 ± 42	204 ± 37
4	531 ± 106	490 ± 97	456 ± 36	466 ± 34	398 ± 42	205 ± 38
5	609 ± 115	553 ± 107	456 ± 36	468 ± 34	400 ± 42	204 ± 37
6	666 ± 127	596 ± 117	456 ± 36	468 ± 34	403 ± 42	206 ± 38
7	666 ± 127	596 ± 117	456 ± 36	468 ± 34	406 ± 42	205 ± 38

$$(c) \text{ Exact CP (4). } (d_1, d_2) = (12, 6). \ p_1 = 7. \ \mathbf{y}[:, i] = \tilde{\mathbf{X}}[:, 0, 1]^2 - \mathbf{X}[:, 0, 0] (\tilde{\mathbf{X}} \text{ is rank-4 CP reconstructed } \mathbf{X}).$$

Rank	rrr	rrrBayes	TTentrywise_CP	TTentrywise_Tucker	TTlowrank_CP	TTlowrank_Tucker
2	376 ± 114	335 ± 98	452 ± 42	463 ± 41	395 ± 47	208 ± 57
3	480 ± 134	427 ± 122	451 ± 41	464 ± 42	395 ± 46	208 ± 57
4	537 ± 153	491 ± 141	451 ± 41	464 ± 42	397 ± 46	209 ± 57
5	609 ± 177	545 ± 153	451 ± 41	464 ± 42	400 ± 46	206 ± 56
6	668 ± 189	591 ± 166	451 ± 41	464 ± 42	403 ± 46	206 ± 56
7	668 ± 189	591 ± 166	451 ± 41	464 ± 42	406 ± 46	209 ± 57

$$(d) \text{ Exact Tucker (4, 4, 4). } (d_1, d_2) = (12, 6). \ p_1 = 7. \ \mathbf{y}[:, i] = \tilde{\mathbf{X}}[:, 0, 1]^2 - \mathbf{X}[:, 0, 0] (\tilde{\mathbf{X}} \text{ is rank-(4,4,4) or rank-(4,4) Tucker reconstructed } \mathbf{X}).$$

Table 5: Out-of-sample RPE (multiplied by 1000 to highlight decimal differences) of various tensor-output regression models trained on synthetic data. Bold font indicates the smallest RPE of a given rank and signal; we use \pm to represent the standard error over 10 repeats.

N Regression coefficients on an EEG dataset

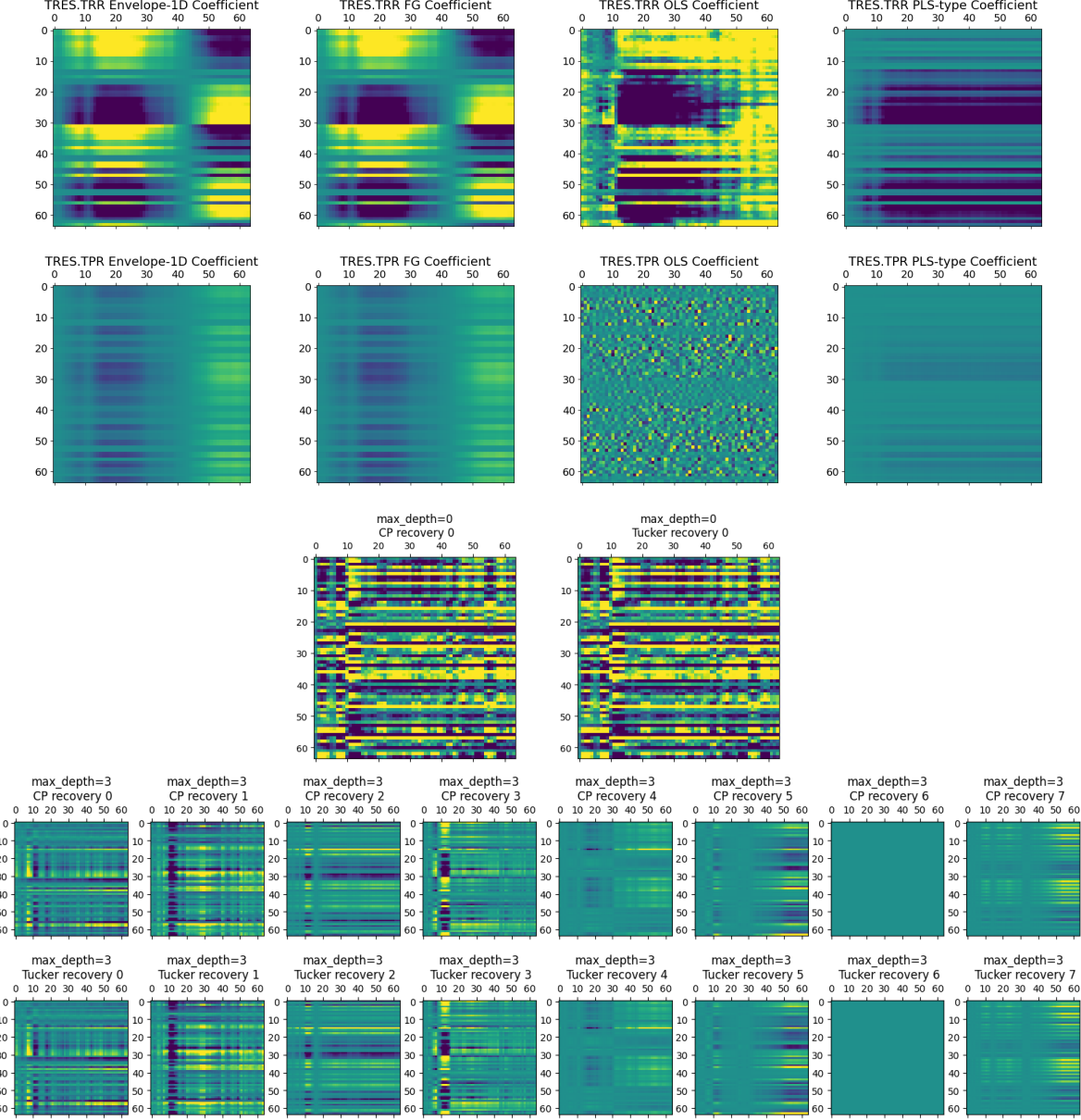


Figure 11: Tensor-input decision tree regression coefficients on an EEG dataset in Zeng et al. (2021). First row: TRES.TRR(1D/FG/OLS/PLS) tensor-response models (following the example in TRES) Second row: TRES.TPR(1D/FG/OLS/PLS) tensor-input models. Third row: coefficients from CP ($R = 5$), Tucker ($R = 5$), Fourth row: coefficients from a tensor-input tree model with depth 3 and leaf node CP models m_j ($R = 5$). Fifth row: coefficients from a tensor-input tree model with depth 3 and leaf node Tucker models m_j ($R = 5$).